2021

ORIGIN AND DISTRIBUTION OF DIFFUSE SOIL CO2 GAS EMISSIONS ACROSS TURRIALBA AND IRAZÚ VOLCANOES, COSTA RICA

Katie Nelson
Michigan Technological University, katen@mtu.edu

ORIGIN AND DISTRIBUTION OF DIFFUSE SOIL CO_2 GAS EMISSIONS ACROSS TURRIALBA AND IRAZÚ VOLCANOES, COSTA RICA

By

Kate M. Nelson

A THESIS

Submitted in partial fulfillment of the requirements for the degree of

MASTER OF SCIENCE

In Geophysics

MICHIGAN TECHNOLOGICAL UNIVERSITY

2021

This thesis has been approved in partial fulfillment of the requirements for the Degree of MASTER OF SCIENCE in Geophysics.

Department of Geological and Mining Engineering and Sciences

Thesis Advisor:	*Chad Deering*
Committee Member:	*Snehamoy Chatterjee*
Committee Member:	*Florian Schwandner*
Department Chair:	*Aleksey Smirnov*

Table of Contents

List of Figures iv

Author Contribution Statement v

Acknowledgements vi

Abstract vii

1 Introduction 1
- 1.1 Geologic Setting 2
- 1.2 Eruptive History 4

2 Methods 5
- 2.1 Soil Diffuse Degassing Measurements 5
- 2.2 Soil Carbon Isotope Measurements 6
- 2.3 Data Analysis 6
  - 2.3.1 CO_2 flux data analysis 6
- 2.4 Error Analysis 7

3 Results 8
- 3.1 Field Observations 8
- 3.2 Diffuse soil gas fluxes and error 11
- 3.3 $\delta^{13}C$ Isotope Populations 15

4 Discussion 19
- 4.1 Turrialba Summit Degassing Evolution 19
  - 4.1.1 Gas Distribution 2013 to Present 19
  - 4.1.2 Carbon Isotopic Signatures 22
  - 4.1.3 Hydrothermal Component: The Ariete Fault 26
  - 4.1.4 Hazard Implications: Turrialba Western Slope 28
- 4.2 Activity between Turrialba and Irazú 29

5 Conclusion 32

6 Future Directions 33

7 Reference List 34

A Error Regression Analysis 38

List of Figures

Figure 1. Turrialba is on the southernmost end of the Central Cordilleran volcanic chain, part of the Central Volcanic Arc, and formed as a result of subduction off the eastern coast of Costa Rica.....3

Figure 2. Full study area with diffuse CO_2 flux point locations. 8

Figure 3. Photos showing each of the six smaller study areas. 10

Figure 4. Log probability plot of soil CO_2 flux measurements plotted with a histogram and normal distribution line of the same. 12

Figure 5. Control point fCO_2 values collected over 13 days of measurement. 13

Figure 6. $\delta^{13}C$ values divided by area in which they were collected. 16

Figure 7. CH_4/CO_2 ratio values calculated from CH_4 and CO_2 concentrations measured over each area, where the green X represents the average value of the atmosphere. 17

Figure 8. Where measurements taken by Epiard et al., (2017) coincide with measurement points recorded in 2021 we calculate the difference in flux from 2013 to 2021. ..20

Figure 9. Comparison between results of a September 2013 diffuse degassing survey over the summit area of Turrialba volcano (background color shading) and the results of transect measurements taken in March 2021. 21

Figure 10. Methane to carbon dioxide ratios plotted against $\delta^{13}C$ over previously defined areas. 23

Figure 11. $\delta^{13}C$ and CH_4/CO_2 measurements at three summit areas from 1998 to 2008 at Turrialba. 25

Figure 12. $\delta^{13}C$ and CH_4/CO_2 ratios for summit 2021 values, 2008 summit values, 2008 Ariete fault values, and 2017 Santa Teresa spring values. 26

Figure 13. Distance between the Ariete fault and soil gas isotopic measurements. 27

Figure 14. $\delta^{13}C$ and CH_4/CO_2 values from the Ariete fault and summit in 2021, values from the summit in 2008, and values from the Sant Teresa Spring collected by OVSICORI (Observatorio Vulcanológico y Sismológico de Costa Rica) in 2017. 28

Figure 15. Well correlated mixing between biogenic and atmospheric source end members, indicated by the dashed line. 30

Author Contribution Statement

The *Soil Carbon Isotope Measurements* portion of the *Methods* section was written by Christofer Jimenez of the Observatorio Vulcanológico y Sismológico de Costa Rica and the National University of Costa Rica. All other sections were completed by the author.

Acknowledgements

I would like to thank Dr. Chad Deering for giving me the opportunity to participate in so many amazing research projects, all of the encouragement, and for the confidence he has in my ability as a scientist. Dr. Florian Schwandner for taking the time to mentor me and to open my eyes to the world of interdisciplinary science. Dr. Snehamoy Chatterjee, for answering my hundreds of questions and teaching me statistical analysis, even when I'm sure it felt like a losing battle. Thank you to the RUMBLE project for allowing this research to be possible, and for the support in the field and in the lab. A huge thank you to Dr. Joshua Fisher and NASA JPL for allowing me to complete a yearlong internship under your guidance, without which I would not be where I am today. My gratitude also to the Michigan Space Grant Consortium for supporting me as a graduate fellow. Finally, my deepest respect and appreciation to my friends and colleagues at Michigan Technological University and to my family back home. Thank you for everything.

Abstract

We characterized large-scale volatile emissions across the summit and flanks of the actively degassing Turrialba volcano, Costa Rica, using soil gas flux measurements and ^{13}C isotopes. The objectives of this study were the following: 1) to monitor changes in the magmatic activity and identify source contributions over Turrialba using measurements of CO_2 soil gas emissions since the volcano last erupted in 2014-2015, and 2) to identify the location and extent of magma at depth, and the structures that allow gas transport to the surface. Degassing at the summit is concentrated along one normal fault lineament, the trace of which runs through the west active crater and fumarolic fields which lay on either side. The high soil gas flux measured, visible evidence of active degassing through fumaroles, and magmatic $\delta^{13}C$ (up to -1.19‰) suggest permeability along this structure that gas follows from magma at depth. $\delta^{13}C$ samples collected in and around fumaroles at the summit are more enriched than those collected within an area known for consistent fumarolic activity in the Ariete fault, which has also been used by previous studies as a baseline for hydrothermal-magmatic $\delta^{13}C$ signatures (~-3‰). Additionally, there is a higher CH_4/CO_2 ratio present in the Ariete fault than at the summit. The difference in isotopic signatures between flank and summit fumaroles is interpreted to indicate magmatic-dominated activity at the summit of Turrialba, possibly comparable to that present at the end of the 2014-2015 eruptive cycle. A similar zone of high diffuse degassing with a more hydrothermal carbon isotopic signature (~-4‰) occurs in the depression between Turrialba and Irazú volcanoes, presenting as a hot spring known as Santa Teresa. We hypothesize the origin of CO_2 flux in this area to be related either to transport through the hydrological system from higher in the volcanic system or from previously unmapped magma at depth below the depression. More detailed mapping of soil CO_2 emissions must be done between Turrialba and Irazú in conjunction with geophysical monitoring to further advance our understanding of the magma distribution and potential magmatic connection between these volcanoes.

1 Introduction

Volcanic systems emit volatiles at varying levels through advective degassing in active plumes or fumaroles and through diffuse soil gas emissions. Carbon dioxide (CO_2) is a primary component of this gas, and the carbon isotopic composition has been shown to reflect the origin and character of degassing on active stratovolcanoes. Volcanic systems exsolve CO_2 at depth which maintains a specific isotopic signature (relative to non-volcanic CO_2) as it rises and reaches the surface. While the primary surface expression of volcanic gas is as often a volcanic vent plume or fumarole, there is a significant anomalous diffusive component which is often more difficult to constrain, and in some cases even greater than any advective component. There is a well-established link between subsurface structures (i.e. faults, fractures, or collapse structures) and diffuse degassing, known as diffuse degassing structures (DDS) (Cardellini et al., 2017; Chiodini et al., 2001; Chiodini et al., 1998; Lin et al., 2019; Melián et al., 2014; Notsu et al., 2006; Viveiros et al., 2020; Werner et al., 2014; and others). Volcanic CO_2 tends to follow DDS rather than being distributed homogeneously across the volcanic flanks, though distributions of diffuse soil gas emissions do not occur at the same rate or evenly along a fault/fracture (Jolie et al., 2016). This behavior has been recorded at Yellowstone volcano, USA (Lin et al., 2019), Campi Flegrei caldera, Italy (Cardellini et al., 2017), and in the East African Rift (Jolie et al., 2019). Epiard et al. (2017) have also shown that diffuse degassing is still a significant contributor to the total carbon budget at Turrialba volcano and others along the Central American Volcanic Arc. Studies have shown that determining changes in the CO_2 flux rate and distribution can improve our understanding of concomitant changes in the subvolcanic magma reservoir that might signal volcanic unrest (Camarda et al., 2012; Melián et al., 2014; Seiler et al., 2017). Increased rates of CO_2 flux (fCO_2), for example, have been correlated with pre-eruptive activity at the El Hierro volcano (Melián et al., 2014) and Etna volcano (Seiler et al., 2017). Additionally, CO_2 flux can provide significant constraints on magma location at depth and constraints on when new material may have been injected (Camarda et al., 2012; Notsu et al., 2006; Werner et al., 2014).

However, where a biological layer exists between the source of gas emissions and the surface there can be mixing between CO_2 of volcanic, biogenic, and atmospheric origin (Chiodini et al., 2008; Malowany et al 2017; Viveiros et al., 2020). Carbon dioxide sources can be roughly distinguished from one another by using a probability plot (Cardellini et al., 2003; Chiodini et al., 1998) or through integrating soil CO_2 flux and carbon isotope measurements (Chiodini et al., 2008; Viveiros et al., 2010). Carbon-13 in CO_2 ($\delta^{13}C$) is well established as a marker of CO_2 origin and has been used with great success as an indicator of changes in source conditions of volcanic systems. For example, levels of hydrothermal-magmatic activity (Moussallam et al., 2014), and separation of biogenic influences on the volcanic gas composition (Chiodini et al., 2008; Viveiros et al., 2020). Chiodini et al., (2008) have shown a clear difference between biogenic and hydrothermal CO_2 at the Solfatara of Pozzuoli volcano. $\delta^{13}C$ has also been used to track changes in the volcanic system at Turrialba periodically throughout the last 20 years. Vaselli et al., (2009) record changes in the isotopic signature across the summit from 1998 until 2008, with Moussallam et al., (2014) measuring in the summit vents in 2013 and Malowany et al., (2017) continuing measurements in 2014. These studies have shown $\delta^{13}C$ to be an effective

indicator of the balance between magmatically-dominated activity and a periodic hydrothermal reservoir, when combined with measurements of other gases or elements (i.e. plume SO_2, He, and CO_2 flux).

Turrialba volcano displays cyclic behavior between hydrothermal-magmatic dominated activity, related to phreatic eruptive activity, and magmatic-dominated activity, related to phreatomagmatic activity. Additionally, De Moor et al. (2016) suggested the existence of two magma reservoirs beneath the volcanic summit, one deep (~8-10 km) and one shallow (~3-5 km). Similarly, at Mt. Etna volcano, Italy, Camarda et al. (2012) showed that peripheral, or flank, contributions to CO_2 flux may be indicative of a deeper magmatic source, whereas measurements at the summit or higher on the volcanic edifice may represent a shallower magma reservoir. This scenario may also exist at Turrialba, and if so, measurements of flank degassing may provide insight to the deep magmatic system once origins of CO_2 flux are well constrained. At the minimum, diffuse gas flux measurements across Turrialba will provide further constraints on magma chamber geometry and magma migration, realities which may have been over-simplified in the past. However, because Irazú volcano is located relatively nearby, measurements of fCO_2 within the depression spanning the two volcanoes may include gas emissions from one of either volcanic reservoir beneath Turrialba volcano, a combination of both, and may include a contribution from the Irazú volcanic reservoir as well.

In this study, we combined measurements of diffuse soil CO_2 emissions, soil isotopic carbon, and CO_2 and CH_4 concentrations, on the Turrialba volcano and through a topographic depression between Turrialba and the Irazú volcano. The objectives of this study were the following: 1) contribute to a characterization of the state of activity within the Turrialba volcanic system, 2) constrain large-scale diffuse degassing over known and unknown DDS both at the summit and on the volcanic flanks, and 3) explore the applications of $\delta^{13}C$ with CH_4 and CO_2 as indicators of CO_2 gas origin especially in areas where volcanic activity is not easily recognized.

1.1 Geologic Setting

Turrialba volcano lies along the Central American Volcanic Arc, created as the Cocos plate is subducted beneath the Caribbean plate at a low angle (Peacock et al., 2005). It is a free-standing andesitic to basaltic-andesitic stratovolcano, located within 10 km of the Irazú volcano, another active stratovolcano of the same arc (Fig. 1) (GVP 2021). Regional faulting trends NW-SE, parallel to subduction, with an additional fault system running perpendicular. Both Turrialba and Irazú formed as part of a pull-apart structure trending SW-NE, creating space within the crust for magmatism that would eventually form both volcanic structures (Montero, 2011).

There are three craters at the summit of Turrialba volcano: West, Central, and East. Of the three, only the West and Central craters have recorded fumarolic activity (Vaselli et al., 2009). These craters are roughly aligned SW-NE, where present activity is concentrated at the West "active" crater. Between Turrialba and Irazú lies a large depression (~10 km wide) attributed to glacial activity (Calvo et al., 2019). Within this valley lies a series of drainages

and cold- and hot- CO_2 springs. Each volcano is known to have an individual magmatic and hydrothermal system, however, there is a possibility that Turrialba and Irazú may share some component of their magmatic plumbing system (e.g. Mt. Saint Helens and Mt. Adams) (Hill, 2009) Therefore, this study investigated not only the summit and flanks of Turrialba and Irazú, but the depression spanning the area between these volcanic massifs.

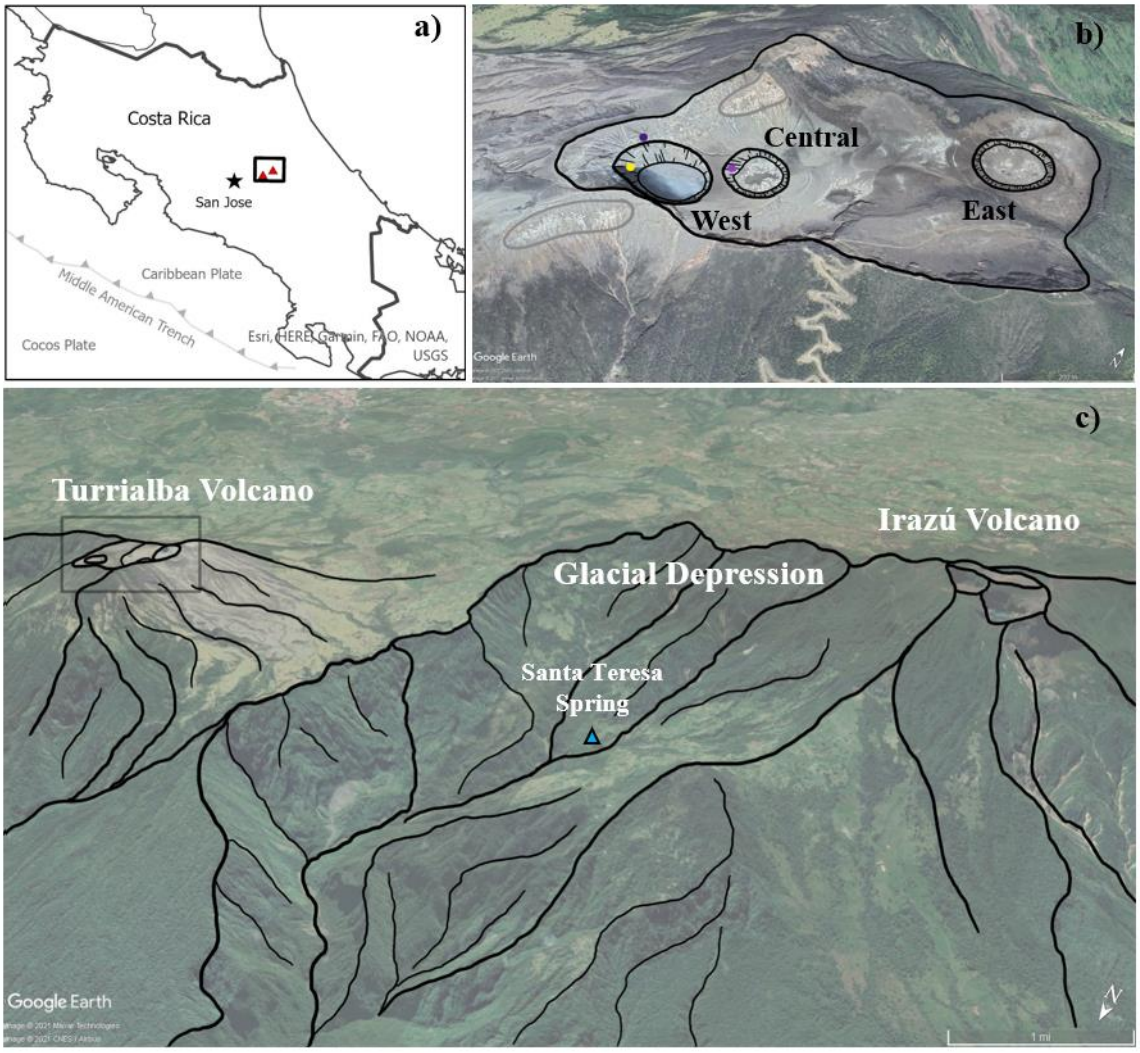

Figure 1. a) Turrialba is on the southernmost end of the Central Cordilleran volcanic chain, part of the Central Volcanic Arc, and formed as a result of subduction off the eastern coast of Costa Rica. b) Three craters make up the volcanic summit; the West, Central, and East. Two fumarolic fields lie to the north and south of the West active crater, outlined in grey. Vaselli et al., (2009) collected samples from the central (light purple point), west (dark purple), and west high temperature (yellow point) fumaroles in 1998-2008. c) Turrialba and Irazú volcanoes are separated by a deep depression, visible from the south. The Santa Teresa spring, discussed in detail below, is located within this area. The dark grey box indicates the summit area of Turrialba volcano.

1.2 Eruptive History

The most notable eruption of Turrialba volcano in recorded history occurred from 1864-1866, after more than 100 years of quiescence. This eruption was characterized by ashfall that reached the Central valley, accompanied by a few pyroclastic flows and lahars (Gonzalez et al., 2015). Activity in the area resumed relative quiescence until fumarolic activity was observed beginning in 1980, with an increase in degassing activity beginning in 1996 (Martini et al., 2010); indicative of reactivation of the volcanic system likely initially related to injection of a small batch of juvenile magma (Campion et al., 2012). Since then, the dominant system has been cyclic, alternating between hydrothermal and magmatic dominated systems (de Moor et al., 2016; Malowany et al., 2017; Martini et al., 2010; Vaselli et al., 2009). Between 1998 and 2008 gas chemistry has indicated a transition from hydrothermally-dominated activity (1998 to late 2001) to hydrothermal/magmatic activity (late 2001 to 2007) to magmatic dominated (2007-2008) (Vaselli et al., 2009). We infer a recharge of the hydrothermal system between 2008 and early 2010, with steadily increasing volcanic activity culminating in a phreatic eruption on 5 January 2010 (Alvarado, 2021). This eruption is indicative of a magmatic-dominated system, coinciding or creating a new vent on the inner wall of the SW crater and allowing open-system degassing to begin (Campion et al., 2012). A second phreatic eruption occurred at Turrialba in 2012 after liquid sulfur was observed pouring from the Quemada fracture (a 4-m wide fracture between the central and southwestern craters, trending roughly NE) and vent incandescence was observed on the Southern wall of the Southwestern crater (Global Volcanism Program, 2013). The 2010 eruption marks renewed eruptive activity at Turrialba which still persists.

Following a period of quiescence, a period of intense phreatic to phreatomagmatic eruptive activity occurred from October 2014 to May 2015, beginning with a blast strong enough to cause the eastern wall of the west active crater to collapse. Two cycles of degassing are evident over the subsequent eruptive activity and are interpreted to be linked to pulses of new magma toward the summit. A hydrothermal gas overprint is evident in the first eruptive phase, but not in the second, suggesting “boiling off” of the hydrothermal reservoir or a change in magma pathways; marking the transition from phreatic to phreatomagmatic activity (de Moor et al., 2016). Summit vent degassing with periodic ash-fall continues to present as part of the ongoing eruptive cycle at Turrialba.

2 Methods

2.1 Soil Diffuse Degassing Measurements

The accumulation chamber method has proven to be an effective tool for measuring diffuse CO_2 gas flux over volcanic flanks (Chiodini et al., 1998; Epiard et al., 2017; and others). We followed the methodology well-established by previous studies to measure CO_2 flux (fCO_2) over 600 points across the flanks of Turrialba and Irazú volcanoes in March of 2021. Two West Systems® flux meters attached to type B accumulation chambers (the larger of two configurations, advantageous for collecting and quantifying high gas flux values) facilitate gas sample flow from the soil-atmosphere boundary within the chamber opening over a LI-COR 820 CO_2 gas analyzer (dynamic range from 0 to 20,000 ppm CO_2 with an accuracy better than 1.5% of reading). The specifications for each fluxmeter used are comparable. Samples are measured as the concentration of CO_2 per second as gas is pumped over a sensor before returning to the sampling chamber (West Systems® Handbook). A "flux", in ppm s^{-1}, is derived from the slope of a best fit line ($R^2 \geq 0.9$) over the course of measurement, which can take >2 minutes at low flux locations. Synchronous measurements of near-surface ground temperature using a Hanna K-type thermocouple at ~15cm depth were collected within 1 m of each point unless ground hardness prevented measurement. Location and elevation values were recorded using a Bad Elf GPS Pro+ where accuracy averaged within 5 m and never exceeded 10 m. Data was collected using the real-time interface between the Bad Elf GPS unit and ESRI ArcGIS Collector offline mapping software. Additional meteorological conditions were recorded, including wind speed and direction using a hand-held Kestrel 3000 wind meter, soil moisture from a Campbell Scientific HydroSense II handheld soil moisture sensor, and barometric pressure and air temperature recorded using internal barometric pressure sensor and thermometer within the Bad Elf GPS, though meteorological conditions remained relatively constant between days of measurement. Control point measurements were taken from the same location at the start and end of each day of field work. These measurements are meant to act as a characterization of variance in flux due to external influence, as we would otherwise expect it to remain relatively stable.

The flanks of Irazú and Turrialba range from agricultural and pastoral fields to natural forest to unvegetated areas of volcanic deposits. Because the study area is so large and heterogeneous relative to a standard study characterizing a single degassing area, a regular geometric measurement grid (which may be preferable for ease of statistical interpolation) is not feasible. Instead, measurement points are guided toward areas of active degassing by known fault maps and the knowledge of local communities, gained through open conversation. In this way, we focus on characterizing areas of high degassing while measuring the spaces between them at a coarse resolution (up to >100 m) as a representation of background CO_2 concentrations. Once an area of interest was identified (for example, over high flux areas such as a fumarolic field or actively degassing hot spring), we collected high-density measurements (as fine as 3 m apart) moving outward until flux and concentration values returned to background or near atmospheric levels.

2.2 Soil Carbon Isotope Measurements

Samples were collected from the 9th to 17th of March 2021 from fumaroles at the summit of Turrialba volcano and from soils on the flanks of Turrialba and Irazú volcanoes. Fumarole gas emissions were sampled by inserting a titanium tube, approximately 2 m in length, into the fumarole to prevent air contamination. Silicon tubing was used to connect the titanium tube to a three-way valve and a 60 ml syringe to extract the gas. The line was cleaned at least three times (extracting and flushing gas with the syringe) before collecting the sample to avoid air contamination. Gas was injected into re-evacuated septum vials (samples of 15ml and 120ml were taken) and overpressurized to ensure successful sample extraction in the lab and minimize air entrainment during transport and storage. At diffuse/soil degassing areas, we collected gas samples by inserting an aluminum tube of approximately 1 m with holes drilled into the lower 30 cm of the tube. Gas was sampled using a 60 ml syringe via a three-way valve. The extracted gas was injected into 15 ml septum vials, after flushing the line three times to avoid air contamination.

Samples were analyzed for carbon isotope compositions of CO_2 and CH_4 on a Picarro G2201-i isotopic analyzer operated in high precision mode at OVSICORI-UNA (Observatorio Vulcanológico y Sismológico de Costa Rica) following the methods of Malowany et al. (2017). Reliable $\delta^{13}C$ values can be achieved on this instrument for analytical CO_2 concentrations between 400ppm and 2000ppm and for CH_4 at 1.5ppm to 20ppm. The samples were extracted from the vials, transferred to 2L flexfoil bags, and diluted using ultra high purity N_2. The flexfoil bag was then connected to the Picarro inlet and analyzed for approximately 10 minutes. Standards were run every 8 samples, including NOAA standard tank containing 1.88 ppm of CH_4 with $ð^{13}C_{CH4}$ of -47.4 ‰ and 394.8ppm CO_2 with $\delta^{13}CO_2$ = -8.3 ‰ (e.g. Caballo-Chaves et al., 2020) as well as an internal standard tank (100% CO_2) with $ð^{13}C_{CO2}$ of -3.8 ‰, which was diluted with UHP N_2 for analysis. Concentration and isotopic average and standard deviation values were recorded from the Picarro software using a ~5-minute data window. Sample data were then corrected using the standard data from the same run, and CO_2 carbon isotope values are reported relative to Pee Dee Belemnite (PDB). Methane concentrations in the samples were typically too low for reliable determination of $ð^{13}C_{CH4,}$ and therefore $ð^{13}C_{CH4}$ values are not reported.

2.3 Data Analysis

2.3.1 CO_2 flux data analysis

Flux values are converted from ppm/s to g/m^2/day to standardize units. This is accomplished by factoring in barometric pressure, air temperature, and accumulation chamber dimensions following the A.c.K equation outlined in the West Systems® handbook:

$$K = \frac{86{,}400 * P}{10^6 * R * T_k} * \frac{V}{A} \quad (1)$$

where P is the barometric pressure in mbar; R is the gas constant of 0.08314510 bar K^{-1} mol^{-1}; T_k is the air temperature in Kelvin; V is the net volume of the chamber, 6.186*10^{-3}

m^3 for a type B chamber like this one; and A is the chamber inlet area which is $3.140 * 10^{-2}$ m^2 for this type B chamber. Dimensions of the flux in mol m^{-2} day^{-1} are found using the following A.c.K.:

$$K = \frac{mol * m^{-2} * day^{-1}}{ppm * s^{-1}} \quad (2)$$

and from here, units can be converted to $g/m^2/day$ using the molar mass of carbon dioxide. A value of 1 was added to all resultant flux values for analysis and removed after calculations were completed. Flux values under the detection limit are assigned a value of 1 and remain in the data set as a representation of areas with very little contribution to flux. However, where our data is compared with those of other studies these values are not considered.

Typically, one would interpret the spatial distribution of the diffuse degassing contribution from a statistical analysis of the space between points. However, the spatial continuity is poor due to the inconsistency and irregularity in measurement spacing. The graphical statistical approach (GSA) was used instead; after the methods of Cardellini et al., (2003). The GSA method partitions fCO_2 data into groups based on the lognormal probability plot, where each group represents a different composition of gas source biogenic, mixed, or volcanic). This method is advantageous in this case as it does not consider spatial correlation within the data.

2.4 Error Analysis

Meteorological variables can potentially influence soil CO_2 flux values as they can change over relatively short time frames and impact soil porosity and diffusion between the soil and atmosphere (Camarda et al., 2006; Chiodini et al., 1998; Hinkle et al., 1994). To identify any confounding influence on gas flux measurements, meteorological variables were recorded synchronously with each flux measurement and treated as predicting variables on fCO_2 in a multivariate analysis. If flux values were significantly impacted, we would expect a statistically significant correlation to become evident. This analysis is made more robust by employing a machine learning component; especially as there is a high likelihood of adding more data points to the model in the future.

3 Results

3.1 Field Observations

The study area can be divided into six sections based on large-scale topography, land cover type, and volcanic activity (Fig. 2).

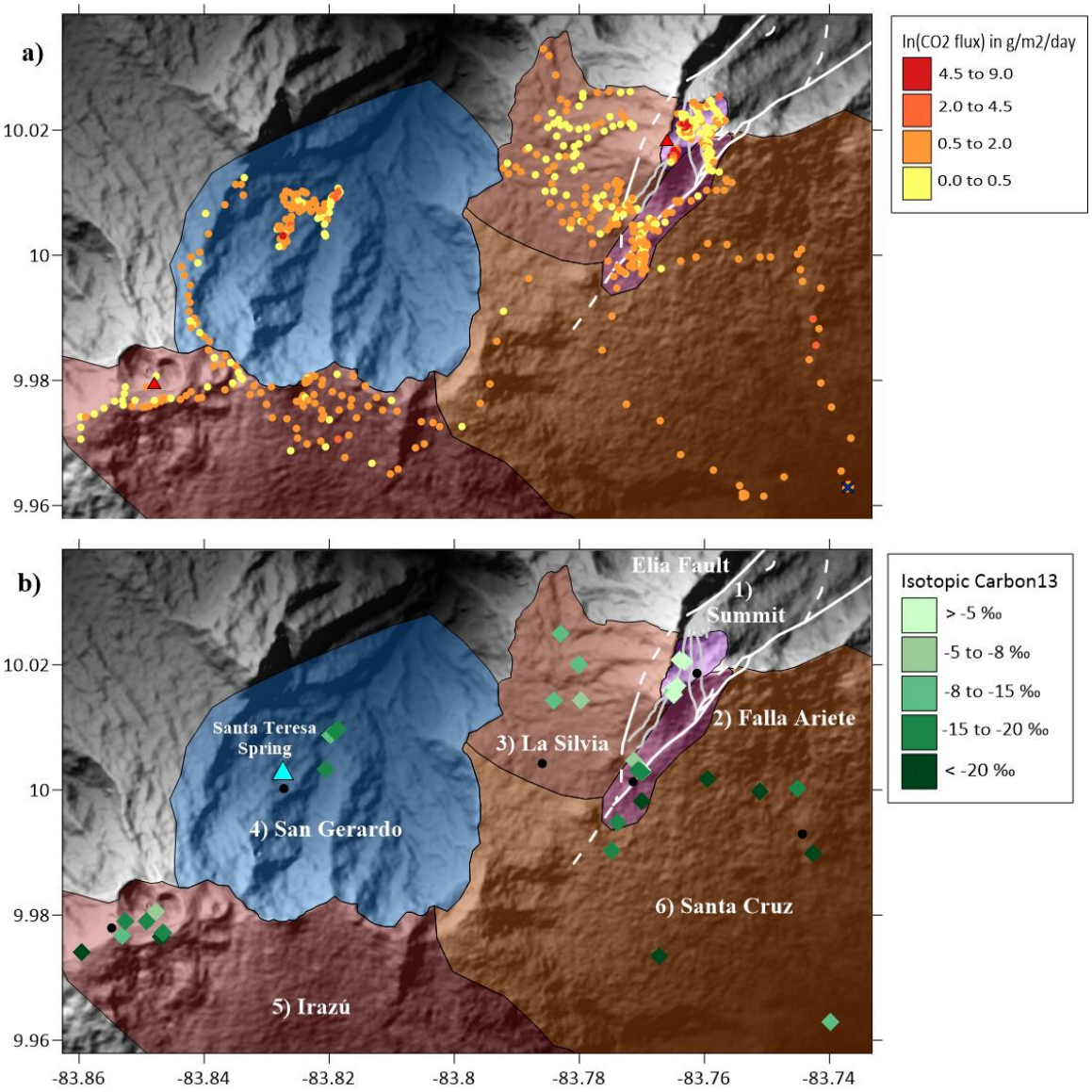

Figure 2. a) Full study area with diffuse CO_2 flux point locations. Dashed lines indicate inferred faults, solid grey lines indicate normal faults, and solid white lines represent strike-slip faults with a normal component (including the Ariete and Elia faults). The summits of both Turrialba and Irazú are indicated by red triangles, and the control point is indicated by a dark blue X. **b)** Full study area with individual areas of analysis indicated by colors and labels. Soil carbon isotope measurements indicated by diamond points. The Santa Teresa Spring is indicated with a blue triangle. Faults remain the same, and are drawn from Calvo et al., (2019). Black dots indicate approximate locations where a photo was taken, as displayed in Figure 3.

In areas 1 (Turrialba's summit) and 2 (the Ariete fault or *Falla Ariete*) gas isotopic composition and CO_2 fluxes indicate a strong magmatic source component. The Ariete fault is also expressed as a fault scarp and intermittent stream, with activity concentrated within fumaroles at the topographic low. Area 3 (La Silvia) is defined by a volcanic ash deposit and dead vegetation. This was the site of mass vegetation die-off beginning in 2005, following the initiation of a summit vent plume on Turrialba. Lethal levels of CO_2 were present in small, localized areas in addition to volcanic plume gas species (predominantly SO_2) carried by persistent trade winds (Global Volcanism Program, 2013; Tortini et al., 2017). Area 4 is characterized by a significant depression where the study area is at least 500 m lower than at any other section and degassing is localized to areas of surface water, including the Santa Teresita hot spring and a series of creeks and rivers. This area is between the Turrialba and Irazú volcanoes. Areas 5 and 6 are defined by predominantly agricultural and pastoral land on the flanks of Turrialba and Irazú. Area 5, known here as "Irazú", is located on the summit and southern flanks of Irazú volcano. We did not measure any significant degassing in this area, allowing any influence from the magmatic system of Irazú to be discounted in this area. Area 6, or "Santa Cruz", is over the Southern and Eastern flanks of Turrialba volcano, excluding the area which is known to contain the actively degassing Ariete fault. Figure 3 displays a visual representation of each area discussed.

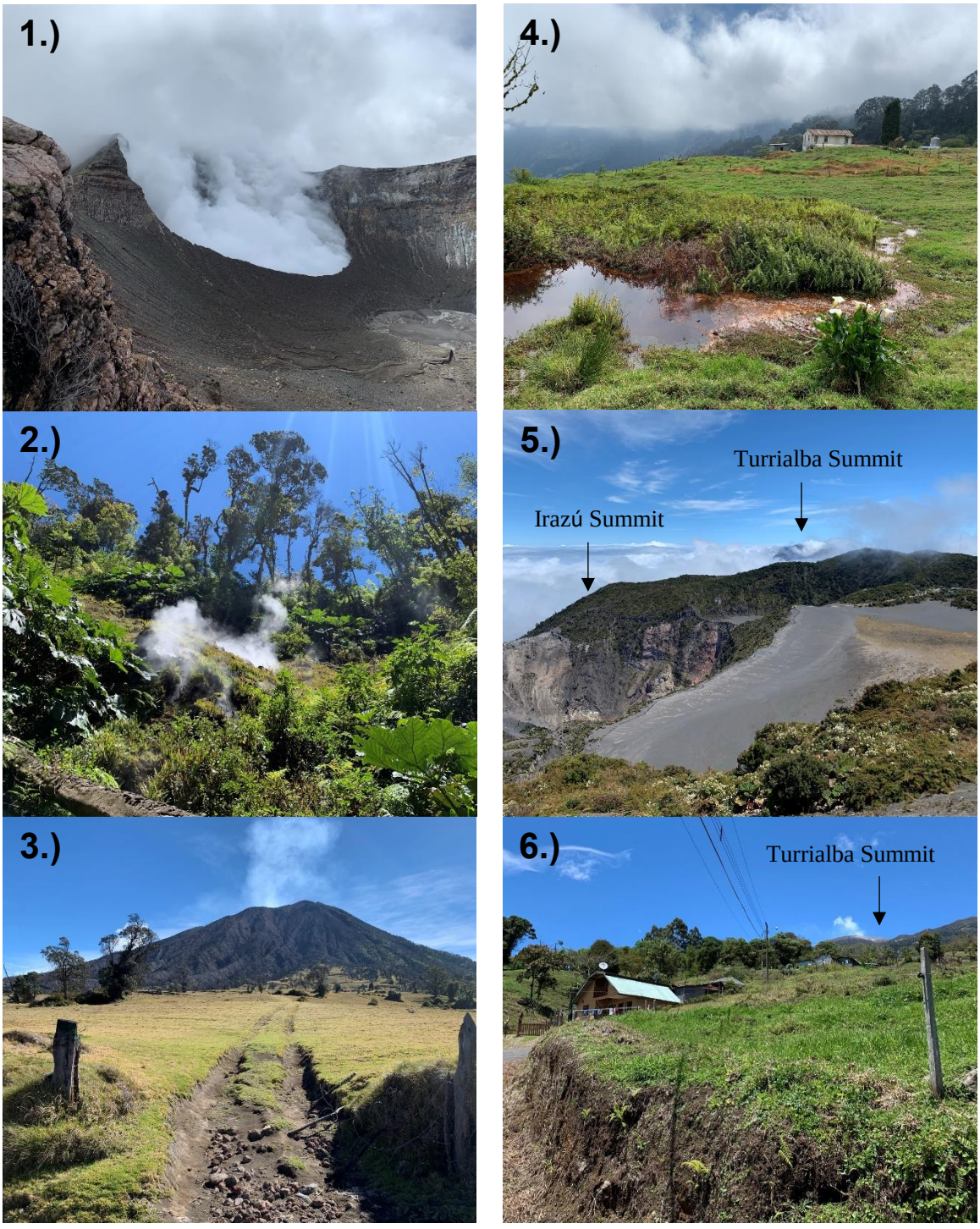

Figure 3. Photos showing each of the six smaller study areas. **1.** Summit of Turrialba facing North toward the Western active crater. **2**. Falla Ariete fumarole facing upward towards the active edges of the fault scarp/drainage. **3**. La Silvia Quemada facing East toward the burned vegetation and summit of Turrialba volcano. **4.** San Gerardo dairy farming community with Santa Teresita hot spring in the foreground. **5.**

Summit of Irazú volcano facing East toward Turrialba volcano. The image itself is from a ridge overlooking the inactive crater, which is to the left and out of sight. **6.** Santa Cruz agricultural community facing North over the flanks of Turrialba toward the summit. Approximate photo locations indicated by black dots in Figure 2.

3.2 Diffuse soil gas fluxes and error

The distribution and range of fCO_2 measurement points between study areas is displayed in Table 1. The minimum of any area is below the detection limit of the sensor, and the maximum of any point was 7917.8 $g/m^2/day$.

Table 1. Results of diffuse degassing measurements by area.

Area	**Number of fCO_2 measurements**	**Maximum values of fCO_2 ($g/m^2/day$)**
Turrialba Summit	82	7917.8
Falla Ariete	110	705.5
La Silvia	119	5.2
San Gerardo	112	540.9
Irazu Volcano	107	7.0
Santa Cruz	70	7.8

Using a lognormal probability plot, we can partition the CO_2 flux data into populations based on the most likely origin of the gas (Cardellini et al., 2003). This approach is widely accepted in areas where both magmatic and hydrothermal systems are degassing in conjunction with a biogenic source of CO_2. We assume the source of CO_2 flux is either magmatic-hydrothermal or biogenic in origin, with the majority of points falling between, where the sources are mixed. Typically, lower fluxes are associated with a biogenic source whereas a higher source is associated with a volcanic origin (Chiodini et al., 1998; Lewicki et al., 2005; and others). Thresholds are determined from a lognormal frequency plot, where flux populations are more easily visualized (Fig. 4). Different populations are defined by bounding inflection points (Sinclair, 1974). Once inflection points are well defined, they can be considered as thresholds. Then, individual measurement can be classified as background, mixed, high, or above the limit of diffuse degassing, therefore classified as advective. Results of this classification are presented in Table 2.

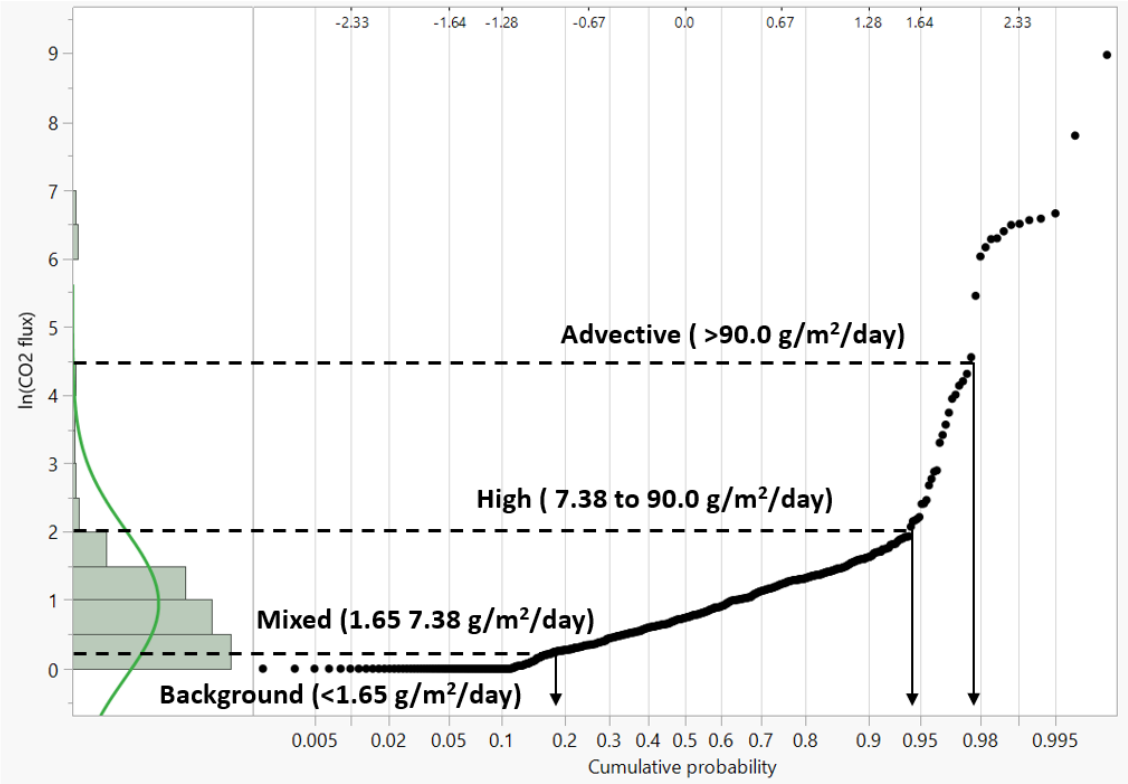

Figure 4. Log probability plot of soil CO_2 flux measurements plotted with a histogram and normal distribution line of the same. Four populations determined from inflection points along this plot are indicated by dashed threshold lines.

Table 2. Flux point statistics, as determined from a cumulative frequency distribution plot (Fig. 4) after Cardellini et al. (2003) and Sinclair (1974).

Population	**Range in ln(grams/m²/day)**	**Percent of Total Points**
Background	≤ 0.5	33.6 %
Mixed	0.5 – 2.0	60.6 %
High	2.0 – 4.5	3.5 %
Advective	4.5 – 9.0	2.3 %

27 measurements of fCO_2 and all meteorological variables were collected at a control point in the morning before field work and in the evening afterward (Fig. 5). Values of fCO_2 ranged from 0.3 g m^{-2} day^{-1} to 5.89 g m^{-2} day^{-1} and averaged at a value of 1.89 g m^{-2} day^{-1}.

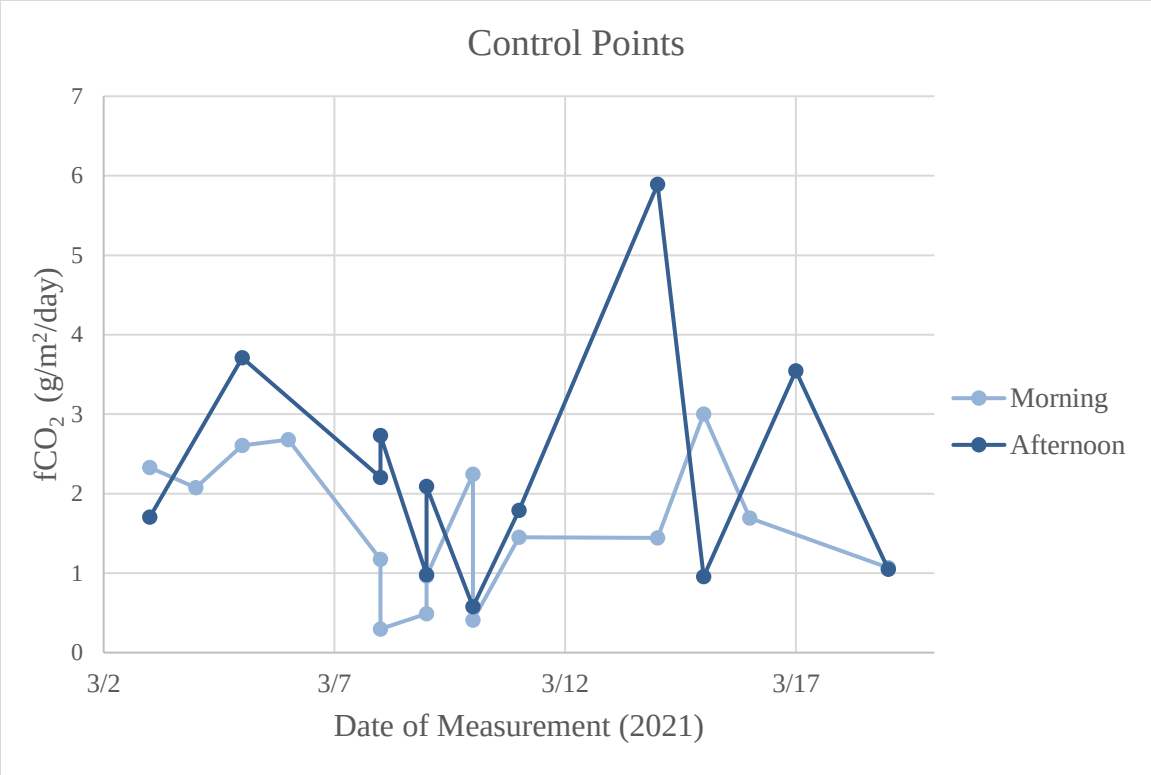

Figure 5. Control point fCO_2 values collected over 13 days of measurement. Light blue measurements were taken before field work, around 7 am, and dark blue measurements were taken in the afternoon after field work, around 4 pm.

Using all fCO_2 measurements over Turrialba that included concurrent meteorological measurements of all conditions, a total of 395, as a training dataset we used 12 multivariate regression models to determine if any measured meteorological conditions significantly impacted CO2 flux. The WEKA machine learning graphic user interface was utilized for ease of analysis (Frank et al 2016). Initially, a filter-based attribute selection was used to ensure variable selection was independent of any algorithm. The *CFS Subset Evaluation* evaluates the worth of a subset of attributes through consideration of predictive ability each secondary variable has on the variable of interest, where more is better, and the degree of redundancy the secondary variables have between each other, where more is worse. The "best" secondary variable is that which has the highest correlation with the variable of interest and the lowest intercorrelation with the other secondary variables (Table 3.). Additionally, the attribute selection was completed using a stepwise regression that results in a ranked list of variables in order of increasing evaluation power. A 10-fold cross validation was used to ensure the data was not overfit by the model.

Table 3. Ranked results of a filter-based attribute selection over the full set of data used from over Turrialba volcano.

Variable	**Rank**
Soil Temperature (°C)	1
Air Temperature (°C)	2
Relative Humidity	3.2
Soil Moisture (VWC)	3.9
Pressure (mBar)	4.9
Elevation (m)	6

Each of 12 regression models were developed to analyze the interconnection between CO2 gas flux and external meteorological variables. Based on the results of the attribute selection that ranked the secondary variables, each model was run six times, each time adding a variable in order of decreasing rank. The best model overall was selected as that which has the highest correlation coefficient and the lowest mean absolute error. Again, a 10-fold cross validation was used in every case to avoid overfitting the model. The best model over these data was a linear regression model using all six variables. The coefficient of correlation is 0.25, and the mean absolute error is 35.67, indicating there is limited predicting power of this model. Full results are displayed in Appendix A-1.

To test the best model trained over the full dataset the 27 measurements at the control point each day of measurement are fed into the same model within the WEKA interface. Using the same model for both data sets avoids any error introduced by normalization that may be created if considering each data set independently, especially as the difference in the number of measurements is so great. The results of this model over the testing data show a coefficient of correlation equaling 0.17 and a mean absolute error of 1.04. This indicates that the model fits the data well but does not provide much significant predicting power. These results are in disagreement with previous studies showing influence on CO2 flux from barometric pressure and humidity, in particular, though these were exacerbated by changes between seasons and diurnally (Chiodini et al., 1998; Hinkle et al., 1994).

We hypothesize that the periods over which we are measuring are relatively short, and so do not adequately capture those variations in meteorological conditions that are great enough to significantly alter the amount of fCO_2. Data over long time-frames, particularly over multiple seasons, would be required to accurately model the influence on fCO_2 measurements. Measurement of the variation related to the diurnal effect on fCO_2 would require analysis outside the scope of this study. It is possible that in low flux areas, such as the control point, small changes in fCO_2 are related to natural variability in the CO_2 diffusion gradient rather than from a significant influence from measured external variables. There is also potential for small variations in soil conditions, or a combination of meteorological conditions, to create variability in fCO_2 between measurement times. If

there is an influence that we are not aware of we stipulate the error would be no greater than 10%, and relative variability in the data would be preserved. For this study, the effect of any meteorological influence not measured are treated as negligible under the assumption that the influence would not be so great as to change the relative population a flux measurement falls within.

3.3 $\delta^{13}C$ Isotope Populations

Isotopic concentrations, in parts per mille (per thousand), were collected over each area during fCO2 measurements. Results of the 53 samples are displayed in Figure 6. with a range of values calculated by Malowany et al., (2017) representing the volcanic end member based on plume samples and fumarole samples taken from Turrialba volcano in 2012. Values of $\delta^{13}C$ fall between -30‰ and 0‰ and are divided by the geographical area they were taken from. The highest $\delta^{13}C$ values collected were from the summit of Turrialba (maximum -1.19‰) and the lowest were collected from the Santa Cruz area (Fig. 6) (minimum -25.91‰). The average error is 1.8‰, with higher error derived from more diluted samples (full data displayed in supplementary material).

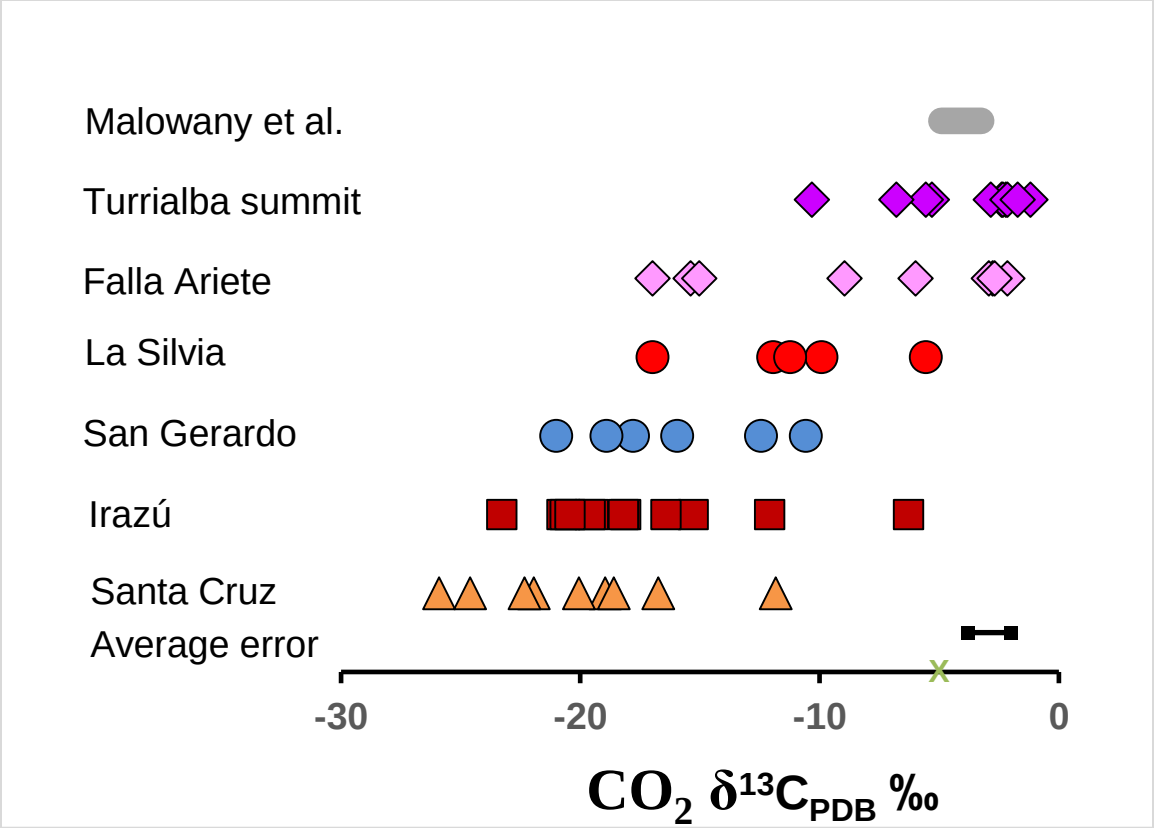

Figure 6. $\delta^{13}C$ values divided by area in which they were collected. Average error is displayed, and green X represents average isotopic concentration of the atmosphere. Full data values presented in supplementary material. Malowany values reproduced from Malowany et al. (2017). Atmospheric $\delta^{13}C$ value derived from NOAA.

Methane gas is a useful tool toward determining carbon flux origins, even as it is impossible to clearly define the origin of methane itself. There are four possible origins of methane emissions in our collected samples: 1) introduction as atmospheric contamination during sample collection; 2) air-saturated ground or meteoric water; 3) production by the activity of microbes or other organisms in the surrounding soil, or 4) introduction by hydrothermal fluid and vapor interactions (Cerling, 1984; Etiope et al., 2006; Giggenbach, 1996). The ratio between CH_4/CO_2 further constrains the origin of gas flux, even as the origin of methane is poorly constrained. The ratio between CH_4 and CO_2 from each sample were calculated from CH_4 and CO_2 concentrations (in ppm). Values range from $2.05E10^{-5}$ at the summit of Turrialba to 0.0044 on the flanks of Irazú, as shown in Figure 7. The average error is 0.001 for these measurements, with higher error from more diluted samples.

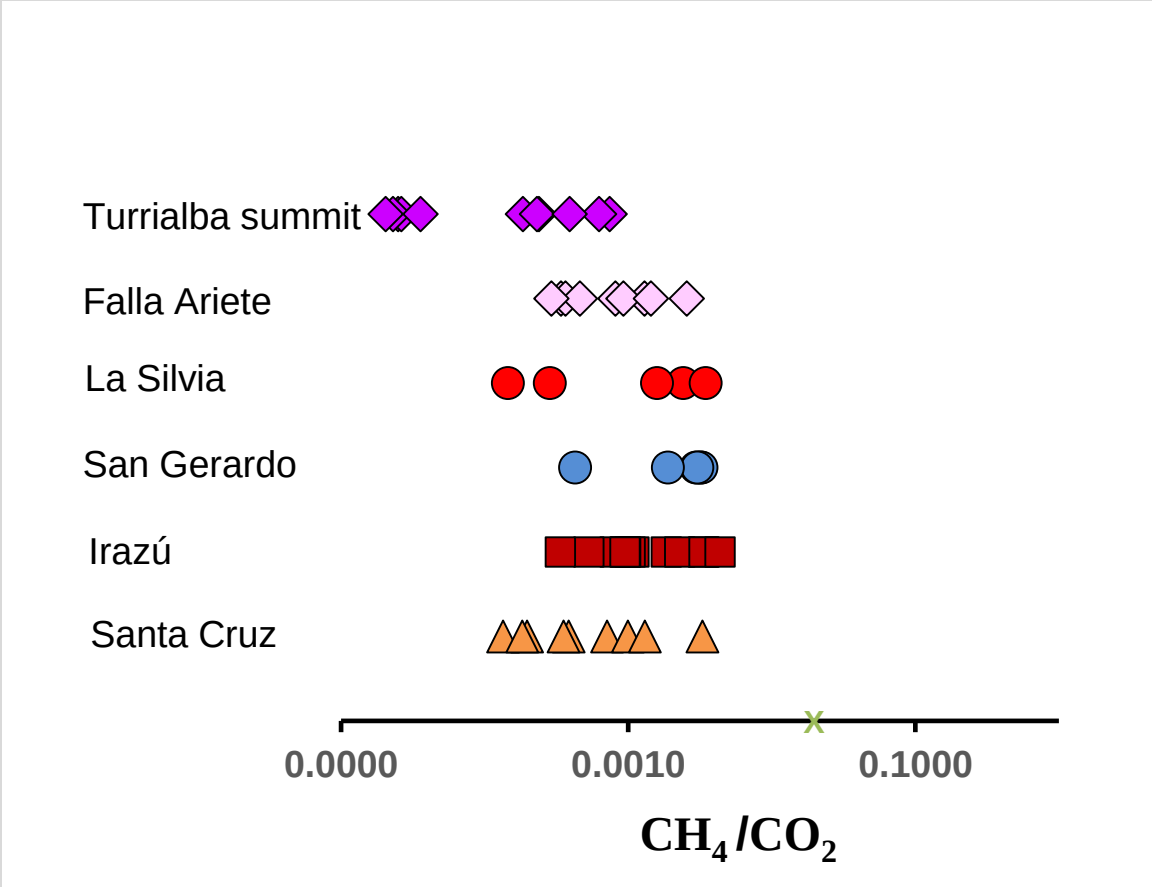

Figure 7. CH_4/CO_2 ratio values calculated from CH_4 and CO_2 concentrations measured over each area, where the green X represents the average value of the atmosphere. Full results are displayed in . Atmospheric value calculated from average global atmospheric concentrations provided by NOAA.

Isotopic values do not show any significant correlation across the dataset either with CO_2 flux values or the commonly used inverse of CO_2 flux values. Because of small scale spatial heterogeneity within CO_2 flux it is possible that though CO_2 isotopes were collected within 1 m of the accumulation chamber this may be a great enough distance to cause a significant change in diffuse degassing. It may be more likely, however, that the origin of CO_2 gas is not directly dependent on the intensity of CO_2 flux present. Assuming this is the case, proportions of each origin of CO_2 gas (indicated isotopically) would remain relatively the same as when CO_2 from the melt mixed with other end members at the source or along ascent. This would explain the lack of any correlation between the amount of degassing (CO_2 flux) and isotopic composition ($\delta^{13}C$). The only exception where we do see a significant relationship is between $\delta^{13}C$ and $1/fCO_2$ over the flanks of Irazú volcano (Fig. 2). Here, there is an R^2 value of 0.61, indicating a significant correlation. There were no values of high flux in this area, the land cover is predominantly agricultural, and isotopic values are generally depleted. Therefore, we suggest that the main driver of fCO_2 is from a biogenic source that has a relatively low contribution from a magmatic source.

There is no generalized correlation between isotopic values and ground temperature or elevation. The lack of correlation between $\delta^{13}C$ and ground temperature is easily explained by a stronger influence from the sun's heat than any subsurface magma, especially where volcanically-derived fCO_2 is not present. Ground temperature does not correlate with fCO_2 until a high flux and high temperature threshold is reached. The actual value will vary between studies and volcanic systems, but the same phenomena is visible across many studies (Lin et al., 2019, Werner et al., 2014). Our primary interest is in diffuse degassing, meaning areas with temperatures and CO_2 flux concentrations above this threshold would likely be outside the scope of this study. Topographic controls on degassing are expected in the study area. For example, areas of high intensity fCO_2 along the Ariete fault are concentrated at the base of a fault scarp, which also acts as an intermittent stream. However, to explore any correlation numerically would necessitate use of relative elevation (or relief) rather than absolute elevation as the study area spans more than 2000 m in elevation.

4 Discussion

4.1 Turrialba Summit Degassing Evolution

4.1.1 Gas Distribution 2013 to Present

Previous studies of soil gas emissions on Turrialba volcano have focused on the summit and the Ariete fault; both areas of known activity and elevated CO_2 emissions. Most recently, Epiard et al. (2017) and others collected 636 soil CO_2 flux measurements over accessible portions of the summit in September 2013. De Moor et al. (2016) provided evidence of a deep magma reservoir (~8-10 km deep) and a shallow magmatic gas source (~3-5 km deep), both of which can have a hydrothermal gas overprint. The hydrothermal reservoir present between the shallow magma reservoir and the summit area of Turrialba is alternately boiled-off and replenished, and magmatic gas does not always travel through the reservoir but rather can bypass it. We postulate that measurements of CO_2 flux at the summit likely represent contributions from both the shallow and deep magma reservoirs, following the conclusions of Camarda et al. (2012). Any changes to summit degassing between 2013 and the present may reflect changes in the geometry of the magma chamber, the permeable pathways gas may travel along toward the surface and/or changes within the magmatic or hydrothermal system. Our measurements across the broader edifice provide insight into the extent of the magmatic system, representing both deep and shallow magmatic CO_2 sources (Camarda et al., 2012).

We completed two days of measurements, resulting in 82 measurement points, over representative cross sections of the summit area to compensate for limited time and access. Three areas were identified as being geologically unique based on historic activity and average intensity and, therefore, were analyzed independently. These are a fumarolic field to the southwest of the west active crater, the central crater, and the eastern crater (Fig. 8). The highest intensity degassing is observed in the west summit crater, recognized as the source of a plume intermittently visible above the volcanic summit. Gas contributions from this area are not considered in this study as emissions are above the limit of the sensor and physically inaccessible.

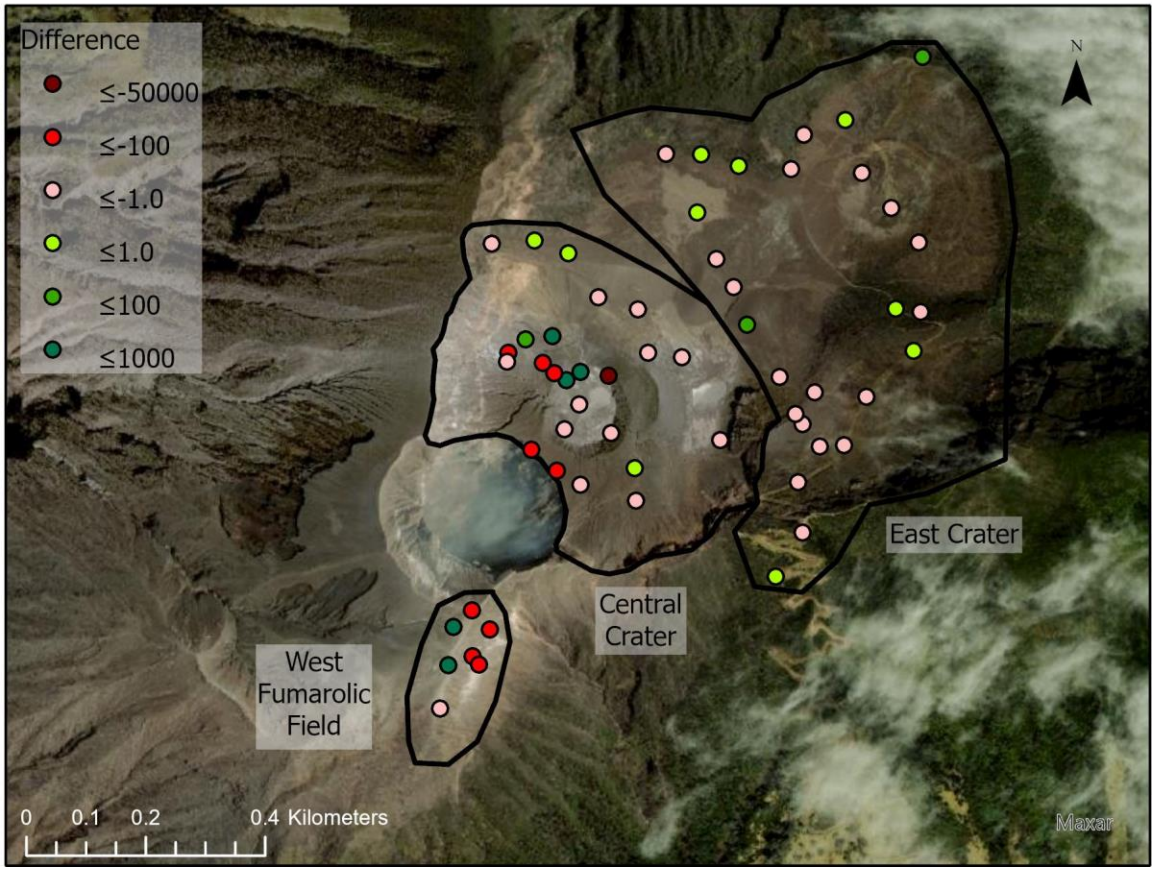

Figure 8. Measurements taken by Epiard et al. (2017) that are located where measurements were made in 2021; change in flux from 2013 to 2021. Differences in flux are displayed as color-coded points across three independent areas on the summit: 1) the west fumarolic field, 2) the central crater, and 3) the east crater.

We use direct comparisons between 2013 and 2021 data collection points within the maximum horizontal accuracy of a standard GPS unit (~10 m) to examine potential changes in the summit gas emissions through time (Table 4.).

Table 4. The results of a change analysis between 2013 and 2021. Data from 2013 provided by Epiard et al., (2017).

Area	Number of points	Average flux 2013	Average flux 2021	Maximum increase	Maximum decrease	Average change
West	7	809.6	904.6	402.3	-1642.0	-275.8
Central	25	2783.5	146.5	777.7	-51564.0	-1984.5
East	27	3.6	1	5.7	-15.3	-1.7

Turrialba has shown significant eruptive activity in the eight years between the Epiard et al. (2017) and present measurement campaigns. Generally, degassing seems to be

continuing along a multi-year trend toward the West-Southwest, leaving the Eastern crater devoid of observable degassing. The average flux over the Eastern crater was low to begin with (3.6 g /m^2/day), suggesting the average decrease in flux since 2013 of 1.7 g/m^2/day to be a significant change. Degassing anomalies at the summit are concentrated along the SW-NE trending lineaments that are part of the Turrialba summit graben (Fig. 9) (Epiard et al., 2017; Montero et al., 2011). Summit structures have been defined as a series of normal faults connecting the Elia fault, which runs along the northern edge of the collapse structure encompassing the NE edge of the Turrialba edifice to the Ariete fault along the southern flank (Fig. 2) (Calvo et al., 2019; Montero et al., 2011). Both the Elia and Ariete faults trend SW-NE, while the connecting faults trend slightly more to the north. Extension and a pull-apart structure opened a pathway connecting mantle-derived melt with the surface, allowing initial formation of Turrialba and Irazú (Montero et al., 2011). Normal motion along a structure has been linked to degassing where rifting is present (Jolie et al., 2019) and over active volcanoes (De Gregorio et al., 2002). Historical motion along the summit normal and strike-slip faults with a normal component suggest the potential for a similar process here, leading to summit degassing features that follow these structures.

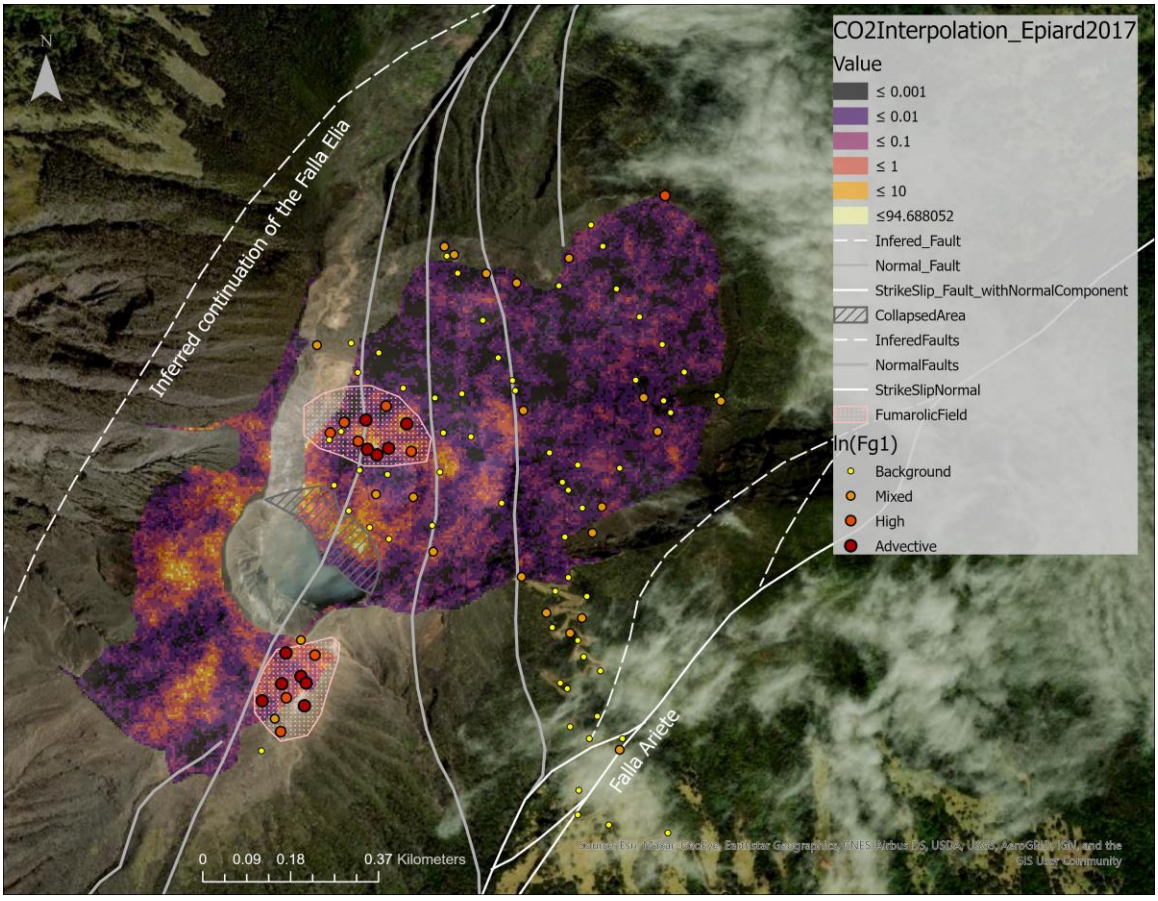

Figure 9. Comparison between results of a September 2013 diffuse degassing survey over the summit area of Turrialba volcano (background color shading) and the results of transect measurements taken in March 2021. All flux data is displayed as the natural log of g m^{-2} day^{-1}. Spatial continuity is captured because of the grid-like spacing present in the 2013 measurements, allowing for the use of a sequential Gaussian simulation

to produce a statistically significant krige map. Data provided by Epiard et al. (2017). Fault map from Calvo et al. (2019).

Since the most recent measurement campaign in 2013, degassing continues to be concentrated along one lineament with fumarolic fields aligned along the northeast and southwest sides of the active west crater. Each unique area of analysis shows a decrease in diffuse degassing, with the greatest change being within the central crater (an average of -1984.5 g m^{-2} day^{-1}). Decreasing diffusive gas flux at the summit overall is likely due to: 1) degassing becoming more channelized, concentrating at the active crater and along this lineament (and in associated fumarolic fields) or, 2) a thick blanket of ash produced by recent eruptions is obstructing gas flow. It is possible that a combination of both is influencing the distribution of gas flow; though more analysis would be required to determine which may be the dominant cause with greater confidence. Additionally, areas along this lineament show evidence of long-term alteration that may lead to greater instability and greater likelihood of collapse in the future. For example, in October 2014 a highly altered area on the western edge of the western crater collapsed to form the larger crater still present today (Epiard et al., 2017).

4.1.2 Carbon Isotopic Signatures

The signature of carbon isotopes collected over the study area shows relative contributions from each of three carbon source end members. Mixing between volcanic, biogenic, and atmospheric sources define the range of $\delta^{13}C$ and CH_4/CO_2 values, all of which are utilized in this study (Fig. 10). Carbon 13 isotopes are often used as an indicator of volcanic activity as they are easily distinguished from carbon 12, which is the primary component of atmospheric carbon species (Chiodini et al., 2008; Malowany et al., 2017; Vaselli et al., 2009; and others). One primary source of ^{13}C globally is from volcanic activity, where atmospheric carbon is considerably depleted in ^{13}C by comparison (NOAA). Because there is almost no $\delta^{13}C$ respired biotically, any ^{13}C present is likely due to volcanic activity or is residual in the atmosphere where there is no significant industrial contribution (Bogue et al., 2019). Atmospheric $\delta^{13}C$ values fall between biogenic and volcanic $\delta^{13}C$, meaning it can be difficult to identify the atmospheric component alone based only on $\delta^{13}C$ values. Methane, and further, the ratio of methane to carbon dioxide in a sample allow further differentiation between atmospheric $\delta^{13}C$, biogenic, and volcanic $\delta^{13}C$ endmembers. Methane concentrations in the atmosphere are higher on average than those present where volcanic or biogenic emissions are dominant. Therefore, samples with high CH_4/CO_2 ratios are expected to have a higher atmospheric component and be “pulled” to the right when plotting $\delta^{13}C$ and CH_4/CO_2 (Fig. 10).

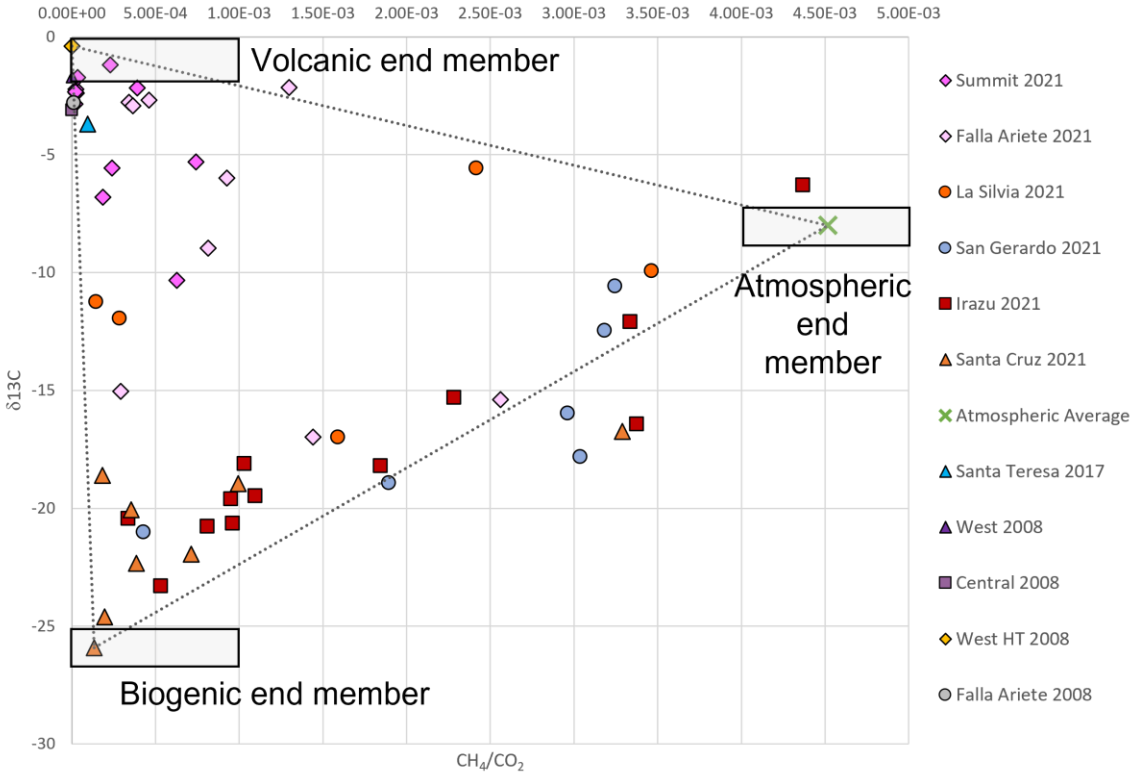

Figure 10. Methane to carbon dioxide ratios plotted against $\delta^{13}C$ over previously defined areas. End members are indicated by boxes where the dimensions of the box are equal to the error along each axis, and determination of each end member discussed below. Grey dotted lines indicate mixing between end members. 2008 data from Vaselli et al. (2009).

Atmospheric $\delta^{13}C$ values are well studied and frequently measured due to their importance for carbon cycle monitoring and tracking of industrial CO_2 output. The isotopic ratio of the atmosphere varies between biomes, seasonally, and diurnally on small spatial scales (NOAA). However, this study uses a generalized atmospheric $\delta^{13}C$ value of -8‰ based on two assumptions. First, because all samples were taken within the same timeframe each day and within the same season any diurnal or seasonal effects would be avoided. Second, Malowany et al., (2017) recorded ambient $\delta^{13}C$ values of -8.3‰ to -10.2‰ in 2014 at Turrialba volcano, which are reasonably close to the average value used in this study. As the isotope samples collected and analyzed in this study were collected from the soil, it is not possible to measure an uncontaminated "true" atmospheric end member. Instead, an average value of atmospheric $\delta^{13}C$ collected by the National Oceanic and Atmospheric Administration (NOAA) is used even as the true atmospheric end member is a range. The same approach is used when finding a representative value of CH_4/CO_2. This was calculated on average for the atmosphere from the average concentration of CO_2 in the atmosphere in 2019 (409.8 ± 0.1 ppm) and the same for methane in 2018 (1.85 ppm). Any confounding influence from industrial CO_2 is considered negligible as the trade winds through this part of Costa Rica are consistently directed west southwest, from the volcano

towards the Central Valley, which contains the only major urban center near Turrialba (Bogue et al., 2019).

Similarly, the biogenic isotopic end member is highly variable depending on ecological conditions, climate, and time of day. Soils have a higher partial pressure than the atmosphere due to the respiration (or release of CO_2) of roots and other microbes in the soil (Cerling, 1984). Much like volcanic CO_2, biotic CO_2 is transported to the surface; though usually at a lower rate. The isotopic composition of organic soil in equatorial climates typically consists of respired CO_2, where $\delta^{13}C$ concentrations usually fall below ~-20‰ (Cerling, 1984; Malowany et al., 2017). Our data falls within the realm of known values, with a biological $\delta^{13}C$ end member of 26‰ to -24‰. While plants are known to produce methane gas, estimates of concentration remain relatively low on a global scale (Houweling et al., 2006). Additionally, where methane gas remains in the soil for long periods and is not facilitated to the surface by high levels of gas flux (such as those form hydrothermal or magmatic systems) it is oxidized by the local ecosystem and not evident at the surface (Tassi et al., 2013). Finally, we expect the concentrations of CO_2 respired by plant photosynthesis to overwhelm concentrations of methane, resulting in a low CH_4/CO_2 ratio where a biogenic source is present.

The magmatic end member composition of $\delta^{13}C$ is variable among individual volcanic systems and through eruptive cycles even within the same system over time (Aiuppa et al., 2014; Malowany et al., 2017; Vivieros et al., 2020). The composition of surface emanations is influenced by both the source magma and overlying hydrothermal system as carbon species rise to the level of volcanic activity. Higher, more enriched values indicate a greater magmatic contribution (Chiodini et al., 2008). Typically, enriched values are representative of melt-derived CO_2 and have $\delta^{13}C$ values above -5‰. The cyclic behavior between hydrothermal/phreatic and magmatic/phreatomagmatic eruptive activity at Turrialba allows us to utilize past studies over periods of well constrained activity to identify the volcanic source end member composition from a time when activity was similar to now (DeMoor et al., 2016; Vaselli et al., 2009). Vaselli et al. (2009) reports $\delta^{13}C$, CO_2 concentrations, and methane concentrations from two summit fumaroles, one high temperature vent, and one fumarole within the Ariete fault, respectively, from 1999 to 2008 (Fig. 1). Their results provide the basis for determining end members within the volcanic system of Turrialba as they collected high-temperature samples where we would expect the least contamination from biological or atmospheric carbon (Aiuppa et al., 2014).

The primary driver of methane production in areas of intense volcanic activity is through generation in the hydrothermal reservoir (Giggenbach et al., 1996; Vaselli et al., 2009). Therefore, we use data from Vaselli et al (2009) over well-constrained active periods to identify a reasonable end member for CH_4/CO_2 in magmatic gas at Turrialba. There is an observable downward trend in CH_4/CO_2 at the west and central craters from 1999 until around 2002, when they determined the system transitioned from a dominantly hydrothermal to hydrothermal magmatic type of volcanic activity. This trend continued between 2002 and 2005, when the hydrothermal system appears to have largely dried out due to the presence of high temperature magma at shallow levels, therefore, shifting the gas composition towards a dominantly magmatic signature (Malowany et al., 2017; Vaselli

et al., 2009). Periods of hydrothermal/magmatic or magmatic-dominated activity have characteristically low CH_4/CO_2 values as the hydrothermal signal is increasingly diluted by magmatic CO_2 input (Giggenbach, 1996). The west high temperature (HT) vent (shown in Figure 1.) shows the same process on an accelerated time scale (Fig. 11). There is a decrease in CH_4/CO_2 as the vent, or high-temperature fumarole, increased rapidly in temperature from 2007 to 2008, which was interpreted as a shallow hydrothermal aquifer boiling off (Vaselli et al., 2009). March 2008 represents the clearest evidence of a "pure" magmatic end member within a period of measurement, and assuming the gas source of the volcanic system has remained stable over time, it is likely a good representation of a "pure" magmatic end member today.

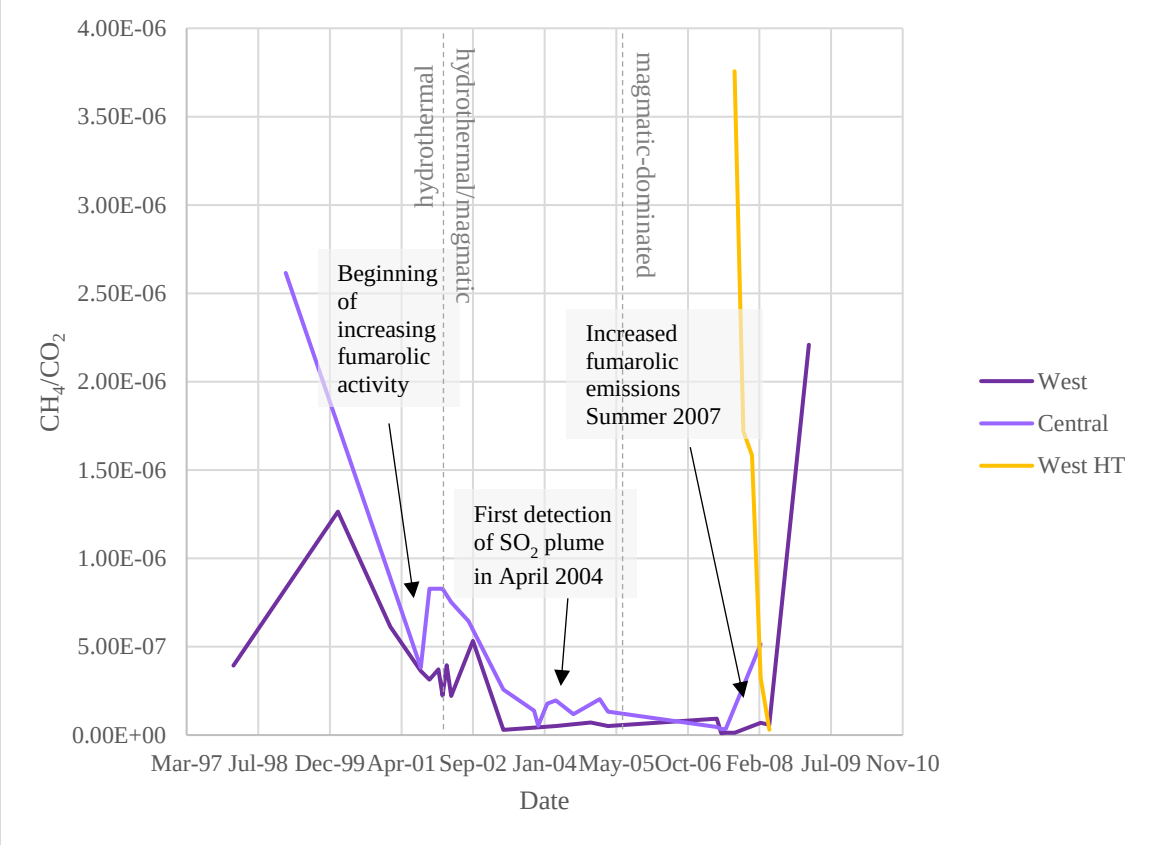

Figure 11. $\delta^{13}C$ and CH_4/CO_2 measurements at three summit areas from 1998 to 2008 at Turrialba. Known eruptive events which may be related to changes in trend are indicated by labels, and the dominant activity over periods of time determined by Vaselli et al., (2009) are indicated with dashed lines. Data from Vaselli et al., (2009).

A comparison between 2008 and 2021 shows a lower CH_4/CO_2 ratio in 2008 than any sample at present (Fig. 12). Additionally, $\delta^{13}C$ is higher at the west HT vent than at any location measured in 2021. Contrary to Vaselli et al. (2009) and other past studies, not all our samples were collected from intensely active areas (i.e., fumaroles), but instead focused on the soil slightly outside of those features. This may introduce some atmospheric contamination and cause $\delta^{13}C$ values to appear more depleted than they may be within the

feature itself (Aiuppa et al., 2014). Nevertheless, isotopic measurements at the summit still suggest a connection with a deep magmatic reservoir. In particular, degassing is concentrated along the SW-NE trending lineament running through the active crater and two fumarolic fields, where the most enriched (volcanic) $\delta^{13}C$ values and highest diffuse CO_2 fluxes are found (Fig. 2). Diffuse soil fCO_2 measurements and $\delta^{13}C$ values are consistent with the conclusion of Epiard et al., (2017) suggesting that there is likely gas flow from depth concentrated along this structure, possibly facilitating further concentration of degassing toward a centralized location.

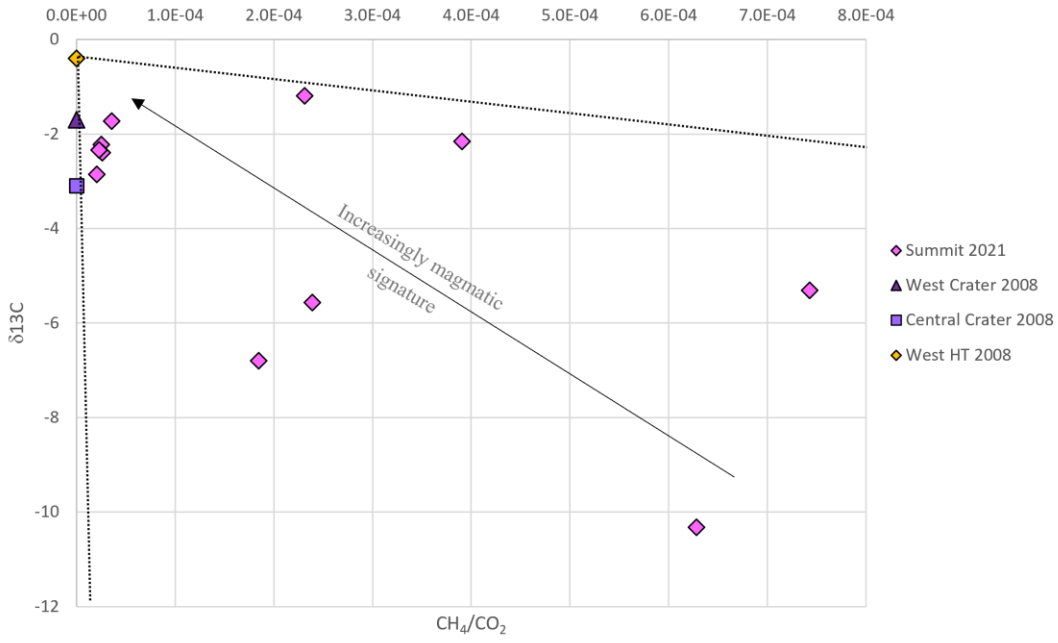

Figure 12. $\delta^{13}C$ and CH_4/CO_2 ratios for summit 2021 values, 2008 summit values, and 2008 Ariete fault values. Dashed lines indicate the ends of mixing lines between the other end members. 2008 values from Vaselli et al. (2009).

4.1.3 Hydrothermal Component: The Ariete Fault

When hydrothermal activity is present at the summit of Turrialba, which it is periodically, it introduces slightly depleted $\delta^{13}C$ values and slightly more elevated CH_4/CO_2 values relative to those that are related to a more magma dominant system. Previous studies have used the Ariete fault fumaroles as an indicator of increased hydrothermal activity relative to the summit (Malowany et al., 2017; Vaselli et al., 2009). Fumarole $\delta^{13}C$ samples, taken from an area known for consistent fumarolic activity in the Ariete fault, retain a consistent d13C signature over many years even as summit $\delta^{13}C$ values are more variable (Table 5.).

Table 5. $\delta^{13}C$ values collected from the Ariete fault over multiple independent measurement campaigns.

Date	$\delta^{13}C$	Reference
Mar-08	-2.8	Vaselli et al., 2009
Sep-13	-2.96	Epiard et al., 2017
Jan-14	-3.33	Malowany et al., 2017
Mar-21	-2.15	This study

The Ariete fault forms a scarp trending SW-NE, significant enough to be visible by satellite, with an intermittent stream at the bottom of a steep valley (40-50 m wide) at the base of the scarp (Fig. 2). Measurements within this valley show high fCO_2 values leading toward advective degassing within the previously mentioned fumaroles. Fumarolic activity culminates at a dry waterfall when moving up the drainage, toward the summit. The zone of elevated gas flux within the drainage, including high soil flux and fumarolic activity, is bounded on either end by steep dry waterfalls. This dry waterfall possibly indicates a tectonic nickpoint, and if so, may also indicate a cross-cutting geologic structure impacting degassing pathways. A similar structure is visible near the southern edge of significant degassing along the Ariete fault. Soil gas isotopic samples taken perpendicular to the Ariete fault show a gradient from enriched $\delta^{13}C$ values toward a more negative, depleted isotopic signature with increased distance from the fault ($R^2 = 0.84$) (Fig. 13).

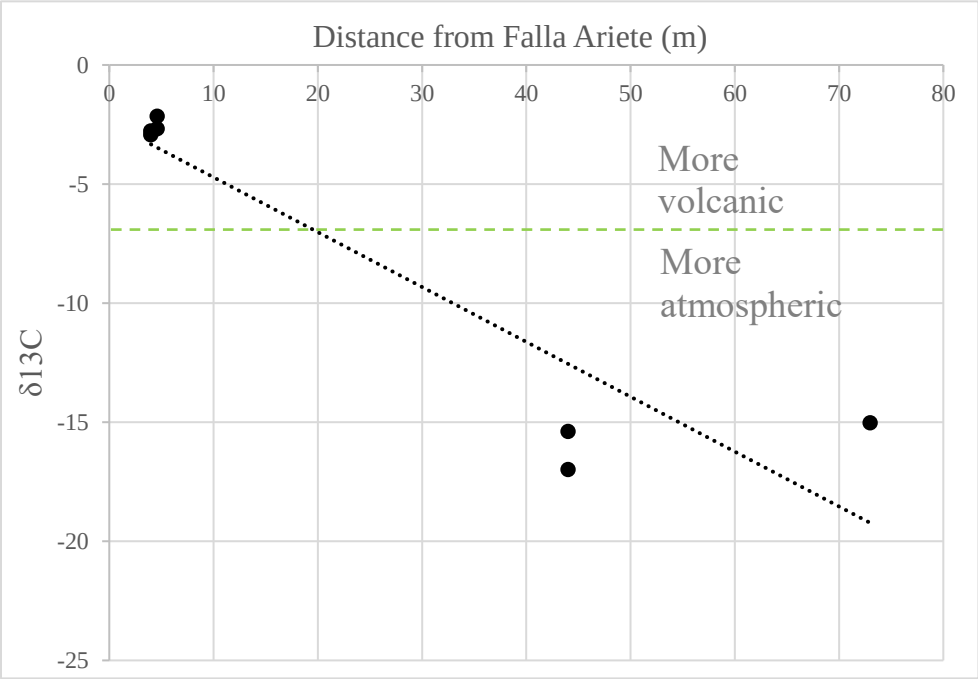

Figure 13. Distance between the Ariete fault and soil gas isotopic measurements. The correlation between increased distance and increasingly negative $\delta^{13}C$ values has a fit of R^2=0.84. Expected error is within the horizontal accuracy of the GPS unit.

Samples taken close to the fault are taken from associated fumaroles and have $\delta^{13}C$ values consistent with hydrothermal activity. They also have higher CH_4/CO_2 ratios than what we

would expect from magmatically-dominated gas (Fig. 14). Giggenbach (1996) determined that magmatic gas would have a very small methane component, if any at all. The presence of higher methane concentrations in the Ariete fault, therefore, are interpreted to indicate the presence of a shallow hydrothermal aquifer contributing to degassing here that is likely independent from activity at the summit.

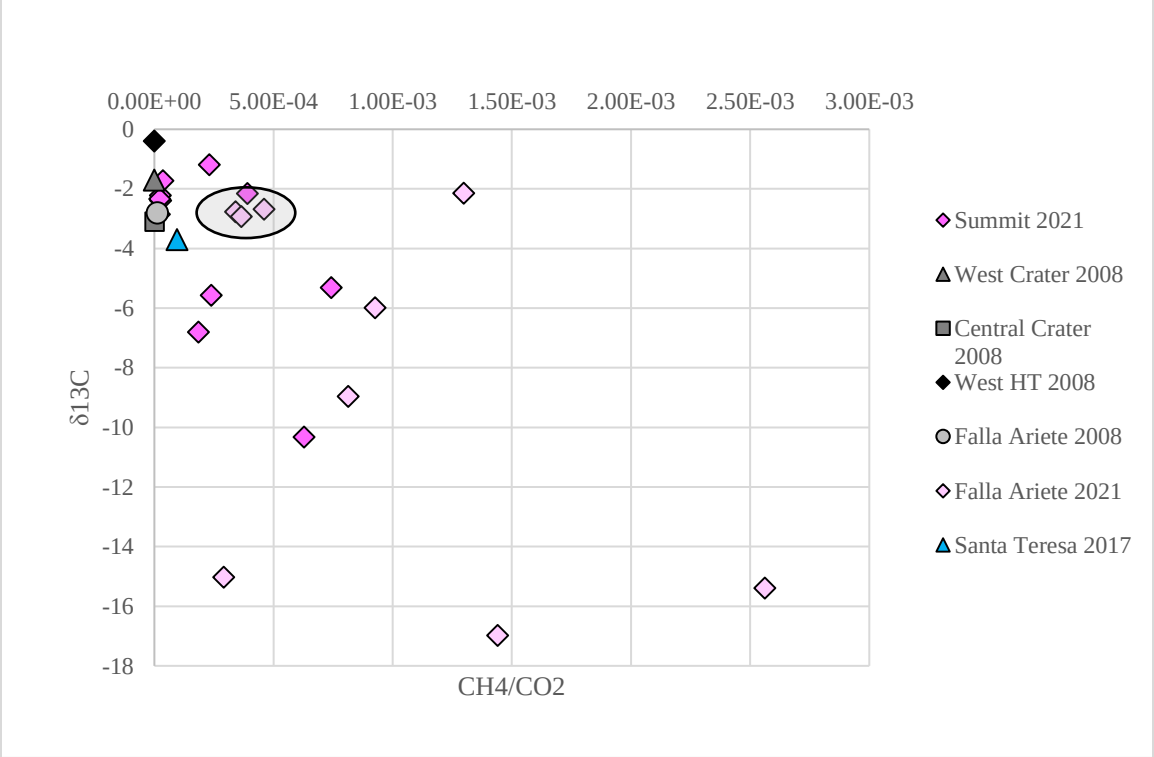

Figure 14. $\delta^{13}C$ and CH_4/CO_2 values from the Ariete fault and summit in 2021, values from the summit in 2008, and values from the Sant Teresa Spring collected by OVSICORI-UNA in 2017. The grey circle indicates those points on the Ariete fault from areas of higher fumarolic activity relative to the rest of the fault.

4.1.4 Hazard Implications: Turrialba Western Slope

On the western slope of Turrialba lies *La Silvia Quemada*, the burned forest, named as such because it is the site of mass vegetation death, caused by strongly elevated soil and plume volcanic gas levels combined with ash fallout since 2004 (Fig. 2) (Tortini et al., 2017). Additionally, there are areas of diffuse degassing so intense that burned vegetation appeared toward the beginning of activity high on the NW flank, but to our knowledge there have been no diffuse soil degassing studies covering this area (Global Volcanism Program, 2013). We record a lack of significant fCO_2 throughout this area, with the lowest values of any area studied (Table 1.). Isotopic signatures and CH_4/CO_2 values fall between all three end members (Fig. 10), making any interpretation of activity difficult. A thick layer of ash covers the entire area, with the potential to reduce gas permeability and subsequently measurable flux. Fumarolic activity was observed, however, just below the outer cone of the active crater near the origin of a 2016 lahar. Field conditions made

measurements in this area impossible, limiting our analysis to a visual recognition of advective degassing. Epiard et al., (2017) have hypothesized a weakening of the upper outer cone, consistent with this observation. Future studies should consider weakening from chemical alteration as a component of hazard monitoring at Turrialba, especially in the scenario where gas is unable to pass through a layer of semi-impermeable ash and instead pools beneath it or is channelized through another structure. If there is a semi-impermeable layer between the subsurface and diffuse degassing measurement equipment it is important for hazard prediction and monitoring to find an alternative method when determining the extent of Turrialba's magmatic activity to the west.

4.2 Activity between Turrialba and Irazú

In exploring the potential connection between Turrialba and Irazú, or if there is an independent presence of magma at depth, we are interested in any diffuse degassing anomalies in the depression between the two volcanoes, the San Gerardo area, or across the flanks of Irazú and Turrialba (the Santa Cruz area) (Fig. 2). The Irazú and Santa Cruz areas have characteristically low flux values, consistent with a lack of known faults or features in either area. There are no documented faults or fractures within the San Gerardo either, and there have not been any diffuse degassing studies in this depression to date. However, there is an actively degassing hot spring (the Santa Teresa spring) and additional warm- and cold- CO_2 springs within the banks of a river that were included in this study. There were anomalously high fCO_2 values associated with all three springs investigated (a maximum flux at Santa Teresa of 540.87g m^{-2} day^{-1}, and maximum fluxes of 232.7 g m^{-2} day^{-1}, 29.5 g m^{-2} day^{-1}, and 34.5 g m^{-2} day^{-1} of three additional springs, respectively).

Isotopic ^{13}C values from San Gerardo fall along a well-defined linear mixing line (R^2=0.8) between biogenic and atmospheric end members, with samples within this trend predominantly being collected from the Irazú, Santa Cruz, and San Gerardo areas (Fig. 15). Initially, this would suggest that these three areas are unlikely to have been influenced by volcanic gas input and instead reflect atmospheric contamination during sampling, which increases with higher dilution of the sample. However, the intensity of CO_2 degassing from the San Gerardo area is inconsistent with a biogenic or atmospheric source. The difference between the isotopic signature and intensity fCO_2 from what we would expect may be related to a greater than normal distance between fCO_2 measurements and isotope sample collections, though unlikely.

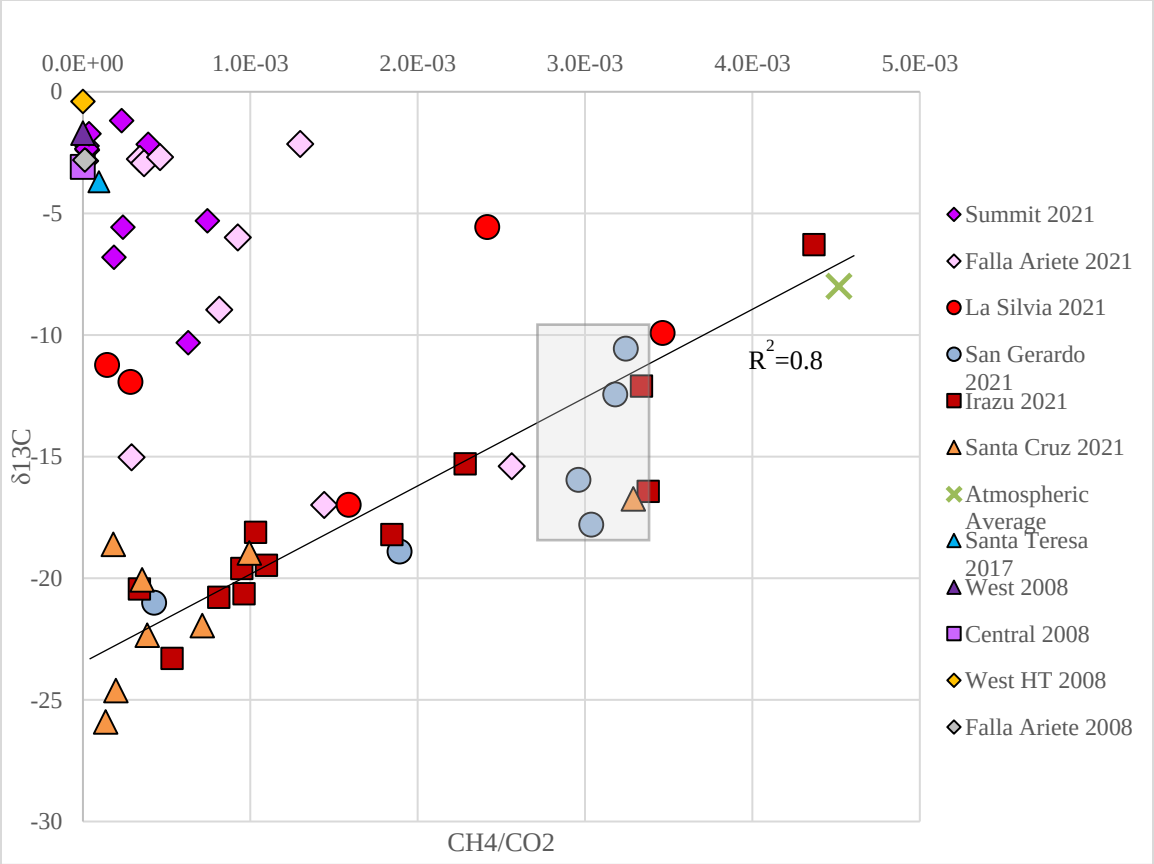

Figure 15. Well correlated mixing between biogenic and atmospheric source end members, indicated by the thin black line. Grey box contains 4 points within the San Gerardo area where high CO_2 flux was present at the isotope sampling location.

Samples collected in-situ from the Santa Teresa spring by OVSICORI in 2017 reflect conditions impossible to measure during the 2021 sampling campaign. This spring has moderate temperatures (~40-50°C) and is characterized by mineral deposits typical of hydrothermal activity, such as hematite and goethite, and red precipitates in the water (location displayed in Fig. 1). Rouwet et al. (2021) obtained chemistry of the water and precipitates from the Santa Teresa spring in 2007, 2009, and 2012. The $\delta^{13}C$ and CH_4/CO_2 values from 2017 fall within a reasonable range of other known hydrothermal activity at Turrialba, such as the Ariete fault (Fig. 14). This is consistent with spring chemistry, indicating steam-heating and near-surface vapor-and-liquid interactions (Rouwet et al., 2021).

There are multiple possible origins for the Santa Teresa hot spring and other CO_2 springs nearby. Their low elevation relative to the volcanic centers of both Irazú and Turrialba and their proximity to an active hydrologic system suggest the possibility that volcanic CO_2 is being captured farther up in the volcanic system and washed down before resurfacing at the base of this depression. Alternately, such high levels of fCO_2 suggest the presence of previously unmapped melt at depth degassing to the surface through a similarly unmapped DDS. This could indicate from the presence of an independent body of magma, or a magma

plumbing system that connects those underlying and directly feeding the Irazú and Turrialba volcanoes. In order to fully evaluate the area, or to determine if there is in fact magma present at depth below the depression, we would need to expand the area surveyed by diffuse degassing measurements and isotopic gas sampling. Collections of water chemistry data, geophysical imaging, and measurements of deformation would also greatly increase certainty when modeling this area and the volcanic systems of both volcanoes.

5 Conclusion

Our investigation of soil diffuse CO_2 degassing has shown the following:

I. Isotopic CO_2 values at the summit of Turrialba reflect those made in past studies (Malowany et al., 2017; Vaselli et al., 2009), and support a deep degassing connection between the lineament of a summit graben and a deep magmatic reservoir (Epiard et al., 2017). Concentrations of $\delta^{13}C$ remain relatively consistent over the years where data are present.

II. The 2014 collapse of the eastern wall into the western crater combined with visual observations of degassing under the edge of the upper outer cone and continued high-intensity degassing in the fumarolic field south of the active crater support inferences that chemical alteration is continuing to destabilize the summit area of Turrialba. Though not recorded in this study, other tectonic structures interpreted as part of the summit graben have potential to begin following the same behavior, with serious hazard implications.

III. Focusing on large-scale diffuse degassing patterns, rather than tightly spaced measurements over a small feature, require a unique set of considerations. The commonly used method of measuring in a grid pattern for applications of a statistical interpolation map is not possible on this scale. Instead, it is more time and cost efficient to concentrate measurements around areas of interest (i.e. mapped faults and features) throughout the study area, with "background" measurements in-between. Maps and past studies are essential to this process, along with the knowledge of those who live and work in the area. Their contributions are crucial when discussing locations and timelines of volcanic activity.

IV. The ratio of methane to carbon dioxide has proven a useful tool toward determining the source mechanism and contribution of diffuse soil CO_2 flux between biogenic, atmospheric, and magmatic end members, with potential to be applied regarding differentiation between magmatic and hydrothermal-magmatic degassing. Because the same analyzer can be used both on CO_2 and CH_4, the ratio between CH_4 and CO_2 has potential act as a cost-effective and convenient alternative to more difficult to sample volcanic gases often used to track gas origin, such as helium or radon. We recommend further analysis include such considerations and test this conclusion across other volcanic systems.

This is the first study at Turrialba volcano where: a) soil gas emissions are considered significantly beyond the crater vent area, helping to distinguish between vent fluxes, fault degassing, and background degassing, and b) measurements were made to investigate a connection between the Turrialba and Irazú volcanic systems across the valley that separates them.

6 Future Directions

Implications from diffuse, elevated CO_2 concentrations emitted by volcanic systems in tropical climates extend from changing physiological processes of tropical trees to allowing the monitoring of subsurface melt as it pertains to eruptive hazards and connectivity between volcanic systems. Future directions would include both of these avenues. Wood carbon isotopes have proven to reflect uptake of volcanic carbon as the tree grows and matures (Bogue et al., 2019). Further constraints on the path of fCO_2 after it is released from the ground and on how much volcanic carbon is absorbed by a tree in a given area allow delineation of CO_2 diffusion and provide insight about terrestrial carbon cycling. The area between Turrialba and Irazú is of particular interest. The presence of elevated fCO_2 from springs throughout the depression imply there is a volcanic source feeding them. Further measurements in this area are essential for understanding if there is melt at depth which could cause future volcanic hazards, and toward determining if Turrialba and Irazú have any connection between their magma reservoirs. Diffuse degassing campaigns are time consuming, and the resolution of the resultant data is often too low to accurately interpolate carbon flux over large areas. Cawse-Nicholson et al., (2019) and others have proven remote sensing indices to show changes in CO_2 flux concentrations over Mammoth Mountain, USA by using the boreal forest as a predictor. Further analysis is required to apply these same techniques in a tropical forest, but the result would be an efficient tool for measuring volcanic CO_2 over large temporal and spatial scales.

7 Reference List

Aiuppa, A., Robidoux, P., Tamburello, G., Conde, V., Galle, B., Avard, G., Bagnato, E., De Moor, J. M., Martínez, M., & Muñóz, A. (2014, 2014/12/01/). Gas measurements from the Costa Rica–Nicaragua volcanic segment suggest possible along-arc variations in volcanic gas chemistry. Earth and Planetary Science Letters, 407, 134-147. https://doi.org/https://doi.org/10.1016/j.epsl.2014.09.041

Alvarado Induni, G. E. (2021). Costa Rica y sus volcanes Editorial UCR.

Bogue, R. R., Schwandner, F. M., Fisher, J. B., Pavlick, R., Magney, T. S., Famiglietti, C. A., Cawse-Nicholson, K., Yadav, V., Linick, J. P., North, G. B., & Duarte, E. (2019). Plant responses to volcanically elevated CO2 in two Costa Rican forests. Biogeosciences, 16(6), 1343-1360. https://doi.org/10.5194/bg-16-1343-2019

Carballo-Chaves, K., Villalobos-Forbes, M., Esquivel-Hernández, G., & Sánchez-Murillo, R. (2020). Isotope composition of carbon dioxide and methane in a tropical urban atmosphere. Isotopes in Environmental and Health Studies, 56(5-6), 624-643.

Calvo, C., Madrigal, K., Merayo, F., Salazar, M., Fallas, C., Alvarado, G. E., Sanchez, B., & Sanchez, R. (2019). MODELO VOLCANOTECTONICO DEL GRABEN CUSPIDAL COMPLEJO DEL TURRIALBA Y SU RELACION CON LOS COLAPSOS SECTORIALES BAJO UN REGIMEN TRANSPRESIVO Y TRANSTENSIVO/VOLCANOTECTONIC MODEL OF THE TURRIALBA COMPLEX GRABEN AND ITS RELATIONSHIP WITH SECTORIAL COLLAPSES UNDER A TRANSPRESSIVE AND TRANSTENSIVE REGIME. Revista geológica de América Central (61), 57. https://doi.org/10.15517/rgac.v2019i61.000

Camarda, M., Gurrieri, S., & Valenza, M. (2006). CO2 flux measurements in volcanic areas using the dynamic concentration method: Influence of soil permeability. Journal of Geophysical Research: Solid Earth, 111(B5), B05202-n/a. https://doi.org/10.1029/2005JB003898

Camarda, M., De Gregorio, S., & Gurrieri, S. (2012). Magma-ascent processes during 2005–2009 at Mt Etna inferred by soil CO2 emissions in peripheral areas of the volcano. Chemical geology, 330-331, 218-227. https://doi.org/10.1016/j.chemgeo.2012.08.024

Campion, R., Martinez-Cruz, M., Lecocq, T., Caudron, C., Pacheco, J., Pinardi, G., Hermans, C., Carn, S., & Bernard, A. (2012). Space- and ground-based measurements of sulphur dioxide emissions from Turrialba Volcano (Costa Rica). Bulletin of Volcanology, 74(7), 1757-1770. https://doi.org/10.1007/s00445-012-0631-z

Cardellini, C., Chiodini, G., & Frondini, F. (2003). Application of stochastic simulation to CO2 flux from soil: Mapping and quantification of gas release. Journal of Geophysical Research: Solid Earth, 108(B9), 2425-n/a. https://doi.org/10.1029/2002JB002165

Cardellini, C., Chiodini, G., Frondini, F., Avino, R., Bagnato, E., Caliro, S., Lelli, M., & Rosiello, A. (2017). Monitoring diffuse volcanic degassing during volcanic unrests: the case of Campi Flegrei (Italy). Scientific reports, 7(1), 6757-6715. https://doi.org/10.1038/s41598-017-06941-2

Cawse-Nicholson, K., Fisher, J. B., Famiglietti, C. A., Braverman, A., Schwandner, F. M., Lewicki, J. L., Townsend, P. A., Schimel, D. S., Pavlick, R., Bormann, K. J., Ferraz, A., Kang, E. L., Ma, P., Bogue, R. R., Youmans, T., & Pieri, D. C. (2018). Ecosystem responses to elevated CO2 using airborne remote sensing at Mammoth Mountain, California. Biogeosciences, 15(24), 7403-7418. https://doi.org/10.5194/bg-15-7403-2018

Cerling, T. E. (1984, 1984/12/01/). The stable isotopic composition of modern soil carbonate and its relationship to climate. Earth and Planetary Science Letters, 71(2), 229-240. https://doi.org/https://doi.org/10.1016/0012-821X(84)90089-X

Chiodini, G., Cioni, R., Guidi, M., Raco, B., & Marini, L. (1998). Soil CO2 flux measurements in volcanic and geothermal areas. Applied geochemistry, 13(5), 543-552. https://doi.org/10.1016/s0883-2927(97)00076-0

Chiodini, G., Frondini, F., Cardellini, C., Granieri, D., Marini, L., & Ventura, G. (2001). CO2 degassing and energy release at Solfatara volcano, Campi Flegrei, Italy. Journal of Geophysical Research: Solid Earth, 106(B8), 16213-16221. https://doi.org/10.1029/2001JB000246

De Gregorio, S., Diliberto, I. S., Giammanco, S., Gurrieri, S., & Valenza, M. (2002, 2002/11/01). Tectonic control over large-scale diffuse degassing in eastern Sicily (Italy) [https://doi.org/10.1046/j.1468-8123.2002.00043.x]. Geofluids, 2(4), 273-284.

de Moor, J. M., Aiuppa, A., Avard, G., Wehrmann, H., Dunbar, N., Muller, C., Tamburello, G., Giudice, G., Liuzzo, M., Moretti, R., Conde, V., & Galle, B. (2016). Turmoil at Turrialba Volcano (Costa Rica): Degassing and eruptive processes inferred from high-frequency gas monitoring. Journal of geophysical research. Solid earth, 121(8), 5761-5775. https://doi.org/10.1002/2016jb013150

Epiard, M., Avard, G., de Moor, J. M., Martínez Cruz, M., Barrantes Castillo, G., & Bakkar, H. (2017). Relationship between Diffuse CO2 Degassing and Volcanic Activity. Case Study of the Poás, Irazú, and Turrialba Volcanoes, Costa Rica. Frontiers in earth science (Lausanne), 5. https://doi.org/10.3389/feart.2017.00071

Etiope, G., Fridriksson, T., Italiano, F., Winiwarter, W., & Theloke, J. (2007). Natural emissions of methane from geothermal and volcanic sources in Europe. Journal of Volcanology and Geothermal Research, 165(1), 76-86. https://doi.org/10.1016/j.jvolgeores.2007.04.014

Frank, Ebie., Hall, Mark A., Witten, Ian H. (2016). The WEKA Workbench. Online Appendix for "Data Mining: Practical Machine Learning Tools and Techniques", Morgan Kaufmann, Fourth Edition, 2016.

Giggenbach, W. F. (1996). Chemical Composition of Volcanic Gases. In R. Scarpa & R. I. Tilling (Eds.), Monitoring and Mitigation of Volcano Hazards (pp. 221-256). Springer Berlin Heidelberg. https://doi.org/10.1007/978-3-642-80087-0_7

Global Volcanism Program, 2013. Turrialba (345070) in Volcanoes of the World, v. 4.10.3 (15 Oct 2021). Venzke, E (ed.). Smithsonian Institution. Downloaded 06 Nov 2021 (https://volcano.si.edu/volcano.cfm?vn=345070). https://doi.org/10.5479/si.GVP.VOTW4-2013

Gonzalez, G., Mora-Amador, R., Ramirez, C., Rouwet, D., Alpizar, Y., Picado, C., & Mora, R. (2015). Actividad histórica y análisis de la amenaza del volcán Turrialba, Costa Rica. Revista geológica de América Central(52), 129-149. https://doi.org/10.15517/rgac.v0i52.19033

Hill, G. J., Caldwell, T. G., Heise, W., Chertkoff, D. G., Bibby, H. M., Burgess, M. K., Cull, J. P., & Cas, R. A. F. (2009). Distribution of melt beneath Mount St Helens and Mount Adams inferred from magnetotelluric data. Nature geoscience, 2(11), 785-789. https://doi.org/10.1038/ngeo661

Hinkle, M. E. (1994, 1994/01/01/). Environmental conditions affecting concentrations of He, CO2, O2 and N2 in soil gases. Applied geochemistry, 9(1), 53-63. https://doi.org/https://doi.org/10.1016/0883-2927(94)90052-3

Houweling, S., Röckmann, T., Aben, I., Keppler, F., Krol, M., Meirink, J., Dlugokencky, E., & Frankenberg, C. (2006). Atmospheric constraints on global emissions of methane from plants. Geophysical Research Letters, 33(15).

Jolie, E., Hutchison, W., Driba, D. L., Jentsch, A., & Gizaw, B. (2019). Pinpointing Deep Geothermal Upflow in Zones of Complex Tectono-Volcanic Degassing: New Insights from Aluto Volcano, Main Ethiopian Rift. Geochemistry, geophysics, geosystems : G3, 20(8), 4146-4161. https://doi.org/10.1029/2019GC008309

Lewicki, J. L., Bergfeld, D., Cardellini, C., Chiodini, G., Granieri, D., Varley, N., & Werner, C. (2005). Comparative soil CO2 flux measurements and geostatistical estimation methods on Masaya volcano, Nicaragua. Bulletin of Volcanology, 68(1), 76-90. https://doi.org/10.1007/s00445-005-0423-9

Lin, P., Deering, C. D., Werner, C., & Torres, C. (2019). Origin and quantification of diffuse CO2 and H2S emissions at Crater Hills, Yellowstone National Park. Journal of Volcanology and Geothermal Research, 377, 117-130. https://doi.org/10.1016/j.jvolgeores.2019.03.002

Malowany, K. S., Stix, J., de Moor, J. M., Chu, K., Lacrampe-Couloume, G., & Sherwood Lollar, B. (2017). Carbon isotope systematics of Turrialba volcano, Costa Rica, using a portable cavity ring-down spectrometer: CARBON ISOTOPE SYSTEMATICS OF TURRIALBA. Geochemistry, geophysics, geosystems : G3, 18(7), 2769-2784. https://doi.org/10.1002/2017GC006856

Martini, F., Tassi, F., Vaselli, O., Del Potro, R., Martinez, M., del Laat, R. V., & Fernandez, E. (2010). Geophysical, geochemical and geodetical signals of reawakening at Turrialba volcano (Costa Rica) after almost 150 years of quiescence. Journal of Volcanology and Geothermal Research, 198(3-4), 416-432. https://doi.org/10.1016/j.jvolgeores.2010.09.021

Melián, G., Hernández, P. A., Padrón, E., Pérez, N. M., Barrancos, J., Padilla, G., Dionis, S., Rodríguez, F., Calvo, D., & Nolasco, D. (2014). Spatial and temporal variations of diffuse CO2degassing at El Hierro volcanic system: Relation to the 2011-2012 submarine eruption. Journal of Geophysical Research: Solid Earth, 119(9), 6976-6991. https://doi.org/10.1002/2014jb011013

Montero, W. (2011). El sistema de falla Atirro-Río Sucio y la cuenca de tracción de Turrialba-Irazú: indentación tectónica relacionada con la colisión del levantamiento del Coco. Revista geológica de América Central(28). https://doi.org/10.15517/rgac.v0i28.7781

Moussallam, Y., Peters, N., Ramírez, C., Oppenheimer, C., Aiuppa, A., & Giudice, G. (2014). Characterisation of the magmatic signature in gas emissions from Turrialba Volcano, Costa Rica. Solid earth (Göttingen), 5(2), 1341-1350. https://doi.org/10.5194/se-5-1341-2014

NOAA. Stable Carbon Isotopes. National Ocean Service website, https://gml.noaa.gov/ccgg/isotopes/c13tellsus.html, accessed on 05/20/2021

Notsu, K., Mori, T., Do Vale, S. C., Kagi, H., & Ito, T. (2006). Monitoring quiescent volcanoes by diffuse CO 2 degassing: case study of Mt. Fuji, Japan. Pure and Applied Geophysics, 163(4), 825-835.

Peacock, S. M., Keken, P. E. v., Holloway, S. D., Hacker, B. R., Abers, G. A., & Fergason, R. L. (2005). Thermal structure of the Costa Rica – Nicaragua subduction zone. Physics of the earth and planetary interiors, 149(1), 187-200. https://doi.org/10.1016/j.pepi.2004.08.030

Rouwet, D., Mora-Amador, R., Ramírez, C., González, G., Baldoni, E., Pecoraino, G., & Inguaggiato, S. (2021). Response of a hydrothermal system to escalating phreatic unrest: the case of Turrialba and

Irazú in Costa Rica. Earth, planets, and space, 73(1), 1-26. https://doi.org/10.1186/s40623-021-01471-8

Seiler, R., Kirchner, J. W., Krusic, P. J., Tognetti, R., Houlié, N., Andronico, D., Cullotta, S., Egli, M., D'Arrigo, R., & Cherubini, P. (2017). Insensitivity of Tree-Ring Growth to Temperature and Precipitation Sharpens the Puzzle of Enhanced Pre-Eruption NDVI on Mt. Etna (Italy). PloS one, 12(1), e0169297. https://doi.org/10.1371/journal.pone.0169297

Sinclair, A. J. (1974). Selection of threshold values in geochemical data using probability graphs. Journal of geochemical exploration, 3(2), 129-149. https://doi.org/10.1016/0375-6742(74)90030-2

Tassi, F., Nisi, B., Cardellini, C., Capecchiacci, F., Donnini, M., Vaselli, O., Avino, R., & Chiodini, G. (2013). Diffuse soil emission of hydrothermal gases (CO2, CH4, and C6H6) at Solfatara crater (Campi Flegrei, southern Italy). Applied geochemistry, 35, 142-153. https://doi.org/10.1016/j.apgeochem.2013.03.020

Tortini, R., Van Manen, S. M., Parkes, B. R. B., & Carn, S. A. (2017). The impact of persistent volcanic degassing on vegetation: A case study at Turrialba volcano, Costa Rica. International journal of applied earth observation and geoinformation, 59, 92. https://doi.org/10.1016/j.jag.2017.03.002

Vaselli, O., Tassi, F., Duarte, E., Fernandez, E., Poreda, R. J., & Huertas, A. D. (2009). Evolution of fluid geochemistry at the Turrialba volcano (Costa Rica) from 1998 to 2008. Bulletin of Volcanology, 72(4), 397-410. https://doi.org/10.1007/s00445-009-0332-4

Viveiros, F., Chiodini, G., Cardellini, C., Caliro, S., Zanon, V., Silva, C., Rizzo, A. L., Hipólito, A., & Moreno, L. (2020). Deep CO2 emitted at Furnas do Enxofre geothermal area (Terceira Island, Azores archipelago). An approach for determining CO2 sources and total emissions using carbon isotopic data. Journal of Volcanology and Geothermal Research, 401, 106968. https://doi.org/10.1016/j.jvolgeores.2020.106968

Werner, C., Bergfeld, D., Farrar, C. D., Doukas, M. P., Kelly, P. J., & Kern, C. (2014). Decadal-scale variability of diffuse CO2 emissions and seismicity revealed from long-term monitoring (1995–2013) at Mammoth Mountain, California, USA. Journal of Volcanology and Geothermal Research, 289, 51-63.

A Error Regression Analysis

Only 395 measurements points were possible to use in the multivariate analysis as they all contained measurements of all variables of interest (results in Table A-1). Points with missing meteorological measurements were not considered in the error analysis. The most common cause of a missing variable is hard ground which is impenetrable to soil temperature and moisture probes. 27 values were recorded at a control point on the southern flanks.

Table A-1. Results of 12 multivariate models over the full dataset used from Turrialba volcano. Results of the best model are highlighted in yellow. C.C. indicates the *Coefficient of Correlation* in this context.

	1-variable		**2-variable**		**3-variable**		**4-variable**		**5-variable**		**6-variable**	
Model	**C.C.**	**Mean absolute error**	**C.C.**	**Mean absolute error**	**C.C.**	**Mean absolute error**	**C.C.**	**Mean absolute error**	**C.C.**	**Mean absolute error**	**C.C.**	**Mean absolute error**
Linear regression (no attribute selction)	0.1955	31.1947	0.1983	32.3438	0.2253	33.0411	0.218	33.4043	0.1669	33.3079	0.2503	35.6721
Simple linear regression	0.1955	31.1947	0.1955	31.1947	0.1955	31.1947	0.1955	31.1947	0.1955	31.1947	0.1955	31.1947
SMOregression (Support vector machine)	0.1774	13.379	0.1797	13.5317	0.1893	13.3482	0.1788	13.4928	0.1316	13.5476	0.1978	13.5234
Additive regression	0.0067	18.2281	-0.0169	18.5113	-0.0064	18.3489	-0.0064	18.3489	-0.004	22.6777	-0.004	22.6777
Bagging	0.143	20.5922	0.1459	20.5774	0.1607	21.1541	0.162	21.2116	0.1633	20.5285	0.1611	20.4746
Regression by Descritization	-0.1689	23.727	-0.1689	23.727	-0.0089	24.3875	-0.0089	24.3875	-0.0089	24.3875	-0.0089	24.3875
ZeroR	-0.1689	23.727	-0.1689	23.727	-0.1689	23.727	-0.1689	23.727	-0.1689	23.727	-0.1689	23.727
Decision Stump	0.1193	18.649	0.1193	18.649	0.1193	18.649	0.1193	18.649	0.1193	18.649	0.1193	18.649
M5P	0.199	30.4536	0.1526	30.047	0.1712	20.9685	0.1117	21.5029	0.108	23.1036	0.1389	20.6928
RandomForest	0.0289	18.0893	0.0298	17.9482	0.0833	18.7258	0.0762	19.2552	0.122	18.5119	0.1496	18.6373
RandomTree	-0.0038	17.3648	-0.0029	18.7058	-0.0047	17.576	-0.0002	16.9414	0.1704	15.341	0.0884	26.8036
REPTree	0.0418	22.7026	-0.0171	23.0442	0.0744	21.9998	0.0744	21.9998	0.074	21.9743	0.074	21.9743